

Radio science observations with Mars Global Surveyor: Orbit insertion through one Mars year in mapping orbit

G. Leonard Tyler,¹ Georges Balmino,² David P. Hinson,¹ William L. Sjogren,³
David E. Smith,⁴ Richard A. Simpson,¹ Sami W. Asmar,³ Patricia Priest,⁵
and Joseph D. Twicken¹

Abstract. Mars Global Surveyor (MGS) radio science comprises studies of the atmosphere and gravity of the planet. Perturbations of the 3.6-cm λ radio path by the atmosphere during periods of atmospheric occultation provide the vertical temperature-pressure structure $T[p(r)]$ to accuracies at the surface of $\Delta T \approx 0.4$ K and $\Delta p \approx 2$ Pa, and ~ 10 K and ~ 0.6 Pa at altitudes of 40–50 km; the error in radius is $\Delta r \approx 1$ m at all levels. Accurate knowledge of the radius permits fixing of the T - p structure to the geopotential and use of the gradient wind equation to calculate components of the wind. Systematic sampling of the atmosphere in combination with the accuracy of the MGS radio system supports studies of the large-scale dynamics of the atmosphere, including seasonal variations of the atmospheric fields and embedded waves such as Kelvin and Rossby waves. Terminator region ionospheric electron density profiles are obtained successfully much of the time but on occasion are undetectable with the MGS system. Two-way radio tracking of MGS with uncertainties in the line-of-sight velocity of several to tens of $\mu\text{m s}^{-1}$ and less supports solution for spherical harmonic models of the gravity field of order and degree in the range of 75×75 , although the degree and order of meaningful terms is limited by the ~ 400 km spacecraft altitude to $\sim 62 \times 62$, corresponding to a resolution of a few degrees of arc on the surface. This resolution of gravity is sufficient to support geophysical studies of the planet's interior structure and history. Additional radio science investigations include the search for gravitational radiation and observation of very low grazing angle forward scattering by the surface of Mars.

1. Introduction

1.1. Overview

Mars Global Surveyor (MGS) radio science (RS) investigations focus on two major areas of study: (1) the gravity field of Mars and its utility for study of the internal structure and history of the planet and (2) the structure and dynamics of Mars' atmosphere and their behavior over time, emphasizing temporal changes in the polar regions for the study of weather, as well as seasonal and interannual variations in climate. Both ar-

reas of study are based on use of a two-part instrument comprising the MGS onboard radio transponder plus elements of the NASA Deep Space Network (DSN) on the ground. As only fundamental observables are recorded at the DSN stations, extensive analysis is required to extract the gravity field and atmospheric conditions from their measured effects on the radio signals. Performance improvements in both the onboard and ground radio systems, first implemented for the failed Mars Observer predecessor to MGS, have produced marked improvements in radiometric data quality and quantity as compared with earlier Mariner and Viking capabilities. At the same time, the low-altitude, nearly circular orbit of MGS provides uniform, fine-scale sampling of the gravity field and systematic, repetitive observations of the atmosphere. In combination with advances in reduction and interpretation techniques for both the gravity and atmospheric observations, as well as comparative studies with other MGS instrument teams, these investigations are providing singular advances in our knowledge of Mars.

In a general way, and in many specifics, the MGS radio science investigations are proceeding along the lines

¹Department of Electrical Engineering, Stanford University, Stanford, California.

²Group de Recherches de Geodesie Spatiales, Toulouse, France.

³Jet Propulsion Laboratory, Pasadena, California.

⁴Goddard Space Flight Center, Greenbelt, Maryland.

⁵Microsoft Corp., Seattle, Washington.

Copyright 2001 by the American Geophysical Union.

Paper number 2000JE001348.
0148-0227/01/2000JE001348\$09.00.

anticipated and planned for Mars Observer. Although the observational strategies have changed in detail, the scientific approach and goals published previously for Mars Observer [Tyler *et al.*, 1992] remain valid. After approximately one Martian year of MGS operation in a mapping orbit at Mars, this paper updates our earlier description of the investigation and describes progress and results to date. This overview is accompanied in this issue by two reports that present topical discussions of results for gravity derived exclusively from radio science observations [Lemoine *et al.*, this issue; Yuan *et al.*, this issue]. Additionally, Hinson *et al.* [2001], who discuss recent MGS results for the atmosphere, should be considered part of this report. Two initial team reports with interpretations were published earlier [Hinson *et al.*, 1999; Smith *et al.*, 1999a]. Background material of direct relevance to MGS radio science can be found elsewhere [Ahmad and Tyler, 1998, 1999; Hinson *et al.*, 1999; Karayel and Hinson, 1997; Konopliv and Sjogren, 1995; Lemoine *et al.*, 1998; Smith *et al.*, 1990, 1993, 1995].

We note the close relationship between these radio science results and those of the MGS Laser Altimeter (MOLA) investigation [Smith *et al.*, this issue]. Zuber *et al.* [2000] derived the first observationally based conclusions regarding the internal structure and history of Mars from a combination of topographic (MOLA) and gravity (RS) results.

In the remainder of this section we discuss in more detail the main features of the radio science investigation and how it is being accomplished. We then discuss

the status of the gravity observations and their utility for understanding Mars' internal structure. Next we describe the occultation measurements of the atmosphere and their relationship to Mars' weather and climate. We include a few remarks on additional scientific observations obtained using the same radio system. Finally, we provide a description of the spacecraft and ground systems being employed in these investigations.

1.2. Radio Science Team

Members of the MGS Radio Science Team (Table 1) are charged with work in the two principal areas described above. Except for a highly stable reference oscillator, The Radio Science Team has no instrument per se onboard MGS but instead shares operational systems with other users of the MGS spacecraft systems and the DSN.

1.3. Operations and Status

1.3.1. Radio science instrumentation.

MGS is the first operational planetary mission to employ exclusively "X-band" technology for radio science observations, tracking, and spacecraft command and communication. The wavelengths used are 4.2 and 3.6 cm, corresponding to 7.2 and 8.4 GHz "uplink" from the ground and "downlink" from the spacecraft, respectively. (An experimental engineering beacon transmits at 0.9-cm wavelength, but this capability has not been applied to the radio science investigation owing to the lack of a suitable operations system on the ground. Lim-

Table 1. Mars Global Surveyor Radio Science Investigation Team

	Affiliation	Function/Investigation
<i>Radio Science Investigation Team</i>		
G. L. Tyler	Stanford University	Team Leader
G. Balmino	Centre National d'Etudes Spatiale	Gravity of Mars
D. P. Hinson	Stanford University	Atmospheric Occultation
W. L. Sjogren	Jet Propulsion Laboratory	Gravity of Mars
D. E. Smith	Goddard Space Flight Center	Gravity of Mars
R. Woo ^a	Jet Propulsion Laboratory	Atmospheric scintillations
<i>Participating Scientists</i>		
J. W. Armstrong	Jet Propulsion Laboratory	Gravitational radiation
F. M. Flasar	Goddard Space Flight Center	Atmospheric dynamics
R. A. Simpson ^b	Stanford University	Mars surface properties
<i>Radio Science Investigation Affiliates</i>		
S. W. Asmar	Jet Propulsion Laboratory	Instrument Engineer
A. S. Konopliv	Jet Propulsion Laboratory	Gravity Analysis
F. G. Lemoine	Goddard Space Flight Center	Gravity Analysis
P. Priest	Jet Propulsion Laboratory ^c	Experiment Rep./Operations Eng.
J. D. Twicken	Stanford University	Data Analysis Software
D.-N. Yuan	Jet Propulsion Laboratory	Gravity Analysis

^aInactive.

^bAlso serves as Experiment Engineer.

^cMGS 1996-2000, now with Microsoft Corp.

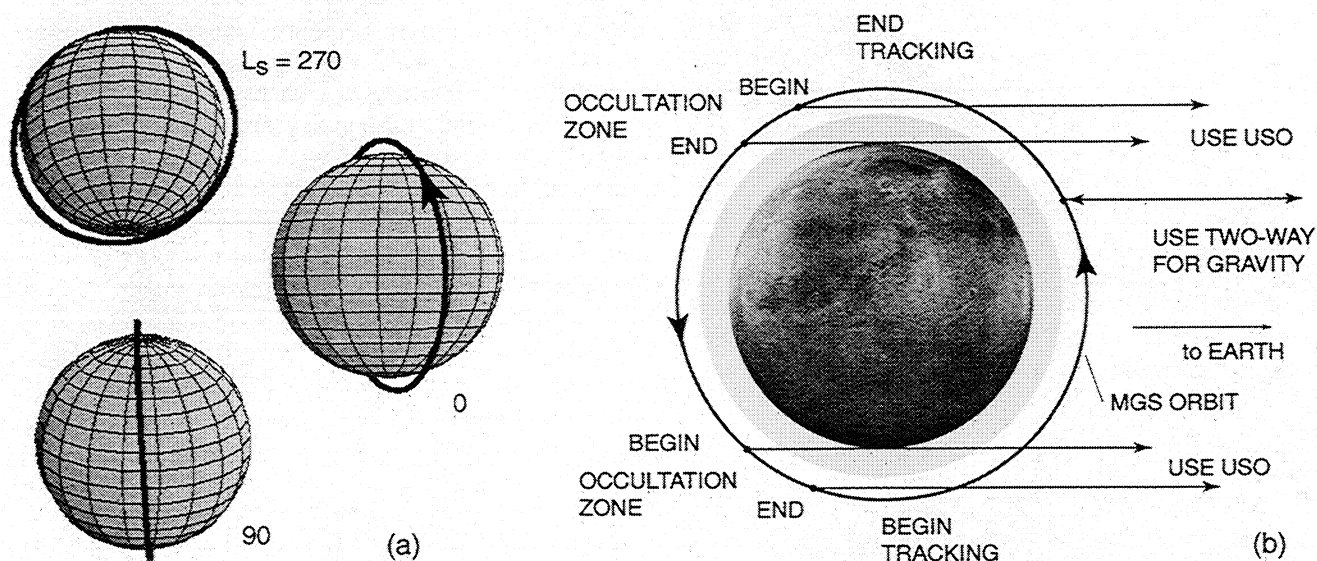


Figure 1. Radio science observations with Mars Global Surveyor. (a) View from Earth during mapping phase at ~ 6 month intervals: December 1999, ($L_s = 270^\circ$), June 2000 ($L_s = 0^\circ$), and December 2000 ($L_s = 90^\circ$) (cf. Figure 2). (b) Observational procedure: Two-way tracking approximately pole-to-pole provides primary data for gravity investigations. One-way observation of propagation effects during occultation periods, when the spacecraft is either moving behind the planet ("immersion") or returning to view ("emersion"), is used to sense the ionosphere and atmosphere. Geometry in (Figure 1b) is schematic.

ited measurements have been carried out by the DSN for engineering test purposes [Morabito *et al.*, 1999.] The ~ 118 -min orbit of MGS is in an ~ 1400 LT plane with respect to the mean position of the Sun, typically providing hourly occultation measurements of the atmosphere in alternate north-south hemispheres of Mars and repeated, dense sampling of the gravity field with varying geometric viewing aspects relative to the orbit plane (Figure 1). Approximately 5000 high-quality radio occultations have been observed to date, primarily in the mapping orbit (see section 1.3.2 and Appendix A).

Key elements of the hardware include (1) the two-way tracking and telecommunications equipment used for command, data return, and navigation, (2) the specialized frequency reference source carried by the spacecraft for radio science purposes and dubbed the "Ultra-Stable Oscillator" (USO), and (3) radio signal sampling and recording equipment on the ground. For gravity investigations, 4.2-cm uplink transmissions from the ground are echoed by the spacecraft radio transponder at a wavelength of 3.6 cm, derived precisely from the uplink. This method of operation is called the "two-way," or "coherent," tracking mode. "One-way," or "non-coherent," spacecraft-to-ground transmissions with frequency derived from the onboard USO are used for occultation measurements of the atmosphere. Perturbations to the one- and two-way signals by the effects of gravity and the atmosphere are detected by comparing the received signal with a hydrogen maser clock on the ground.

The use of the MGS radio system for scientific purposes has proceeded in a manner similar to that for past missions [see, e.g., Tyler, 1987]. The radio signals are affected by the gravitational influence of the planet on the motion of the spacecraft, by the medium through which the signals travel, and by performance of the various systems involved on both the spacecraft and the ground. For study of either Mars' gravity or atmosphere the primary observation is of variations δf in the frequency f_0 of the signal propagating between the spacecraft and ground antennas. The change in frequency provides the apparent line-of-sight velocity of the spacecraft relative to the tracking station through the Doppler effect. Perturbations of the radio signal thus provide information on the spacecraft trajectory, for gravity, and on the atmosphere, in the case of occultation measurements. A secondary quantity of interest for the gravity investigation is the spacecraft "range," or the distance between the spacecraft and the ground tracking station. In this instance the observable is the propagation time required for radio signals to travel round-trip from the ground antenna to the spacecraft and return, which is scaled to find the round-trip path length. Range can be obtained simultaneously with the frequency measurements during periods of two-way tracking. With MGS we obtain these measurements at levels of accuracy corresponding to line-of-sight errors characteristically of the order of $10 \mu\text{m s}^{-1}$ for velocity and a few meters for range (section 6.2). The capability of DSN equipment to measure signal amplitude fluctuations during atmospheric occultations at precisions of a few percent is useful in remov-

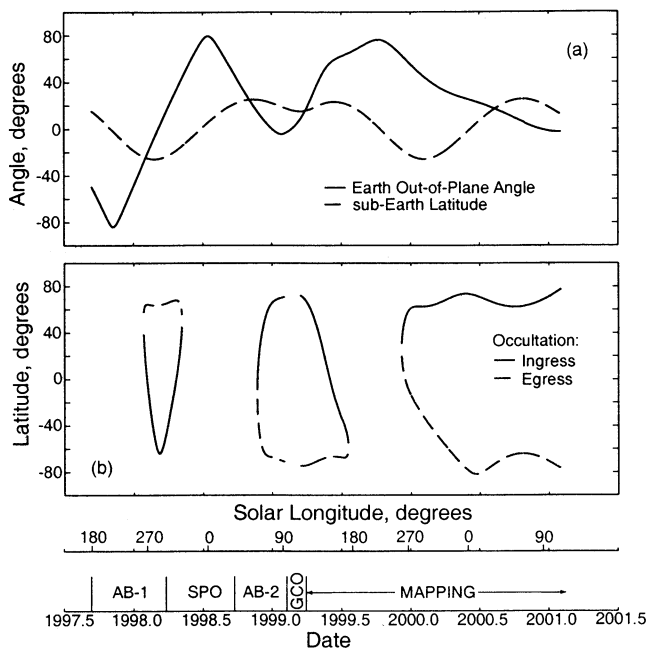


Figure 2. Geometry of radio science observations. Lower scale indicates mission phases (see text). (a) Observational conditions: Sub-Earth latitude and angle of the Earth-Mars line-of-sight measured from the orbital plane; angle is positive for Earth-to-Mars line west of the MGS orbital plane. (b) Latitude of Earth occultation points: In the mapping orbit, there are no occultations during periods when the orbit plane opening angle is greater than $\sim 64^\circ$.

ing diffraction effects and improving vertical resolution in those results. Prior to MGS it was anticipated that intensity scintillations associated with atmospheric turbulence might be detectable in the MGS measurements. To date, however, no intensity scintillations have been observed.

1.3.2. Geometry and coverage. Radio science observations have been obtained almost continuously following MGS launch. During interplanetary cruise to Mars, data were collected for purposes of evaluating and understanding the overall radiometric performance of the operations systems involving both spacecraft and ground. In addition, cruise data were collected for a period of ~ 3 weeks in a search for gravitational radiation (section 4.2).

MGS entered a Martian orbit on September 12, 1997. The first ~ 18 months of orbital operations were used to circularize the orbit in two Aerobraking Campaigns (AB-1 and AB-2) bracketing a Science Phasing Orbit (SPO), which itself was approximately centered on solar conjunction (Figure 2). Radio tracking during aerobraking was used primarily for orbit determination and control; the gravity signatures in these data are all limited to high altitudes by operational exclusion of tracking data within 30 min of periapsis, and consequently have been less useful for science. On the other hand, when occultation measurements could be sched-

uled during aerobraking, good atmospheric profiles were obtained (January–April 1998, December 1998 to January 1999). Aerobraking was suspended for solar conjunction and orbit phasing in 1998; during this time, periapsis precessed from 60°N across the north pole and back to 60°N at an altitude of ~ 170 km, providing gravity data with some of the highest spatial resolution of the mission. MGS entered the final mapping orbit in early February 1999. Premapping instrument calibrations, including ~ 23 days of almost continuous tracking for determination of a preliminary gravitational model, the Gravity Calibration Orbit (GCO), ended in early March. Mapping operations began on March 9, 1999.

The basic features of the Mars-Earth-spacecraft geometry in the mapping orbit mission phase are given in Figures 1 and 2. Figure 1 includes the view of the mapping orbit from Earth and the strategy for sharing the orbit between occultation studies when MGS is near the limb of the planet and gravity studies during the MGS Earthside pass. Occultation measurements are routinely carried out with the spacecraft transmitter referenced to the onboard USO; the change from normal tracking and telemetry transmission to the USO and back again is sequenced either by programmable delays from the start of solar occultation or, when in β -supplement mode, preprogrammed from the ground [Albee *et al.*, this issue]. Sensing of the gravity field occurs during all tracking periods in which the spacecraft is visible from Earth exclusive of the occultation periods.

Figure 2a shows the variation of the orbit opening between the time of orbit insertion and the end of the primary MGS mission in early 2001. Extremes for the mapping orbit occur when Earth is near quadrature with respect to Mars. Although the orbit is fixed with respect to mean solar time on Mars, there is considerable variation in the viewing aspect from tracking stations on Earth (see Figures 1 and 2). In particular, the out-of-plane angle reaches values near $+80^\circ$ about five months after opposition, when the orbit orientation is nearly “face-on” and the spacecraft can be viewed continuously. In contrast with extreme out-of-plane viewing, the orbit is viewed edge-on ~ 5 months prior to opposition. These changes in geometry modulate the sensitivity of line-of-sight tracking data to the gravity field; at the time of orbit plane crossing the line-of-sight accelerations represent most strongly the in-plane orbit perturbations, while the face-on geometry yields the cross-track perturbations most directly. Also shown in Figure 2a is the variation of Earth’s declination with respect to Mars’ equator, which changes roughly with the Martian year. The obliquity of Mars’ rotation axis allows MGS to be tracked over the polar regions during alternate Martian seasons, as indicated by the varying declination of Earth.

Figure 2b gives the latitude of the occultation points over time. Observational opportunities are confined to periods within the lateral extremes of the closed loops.

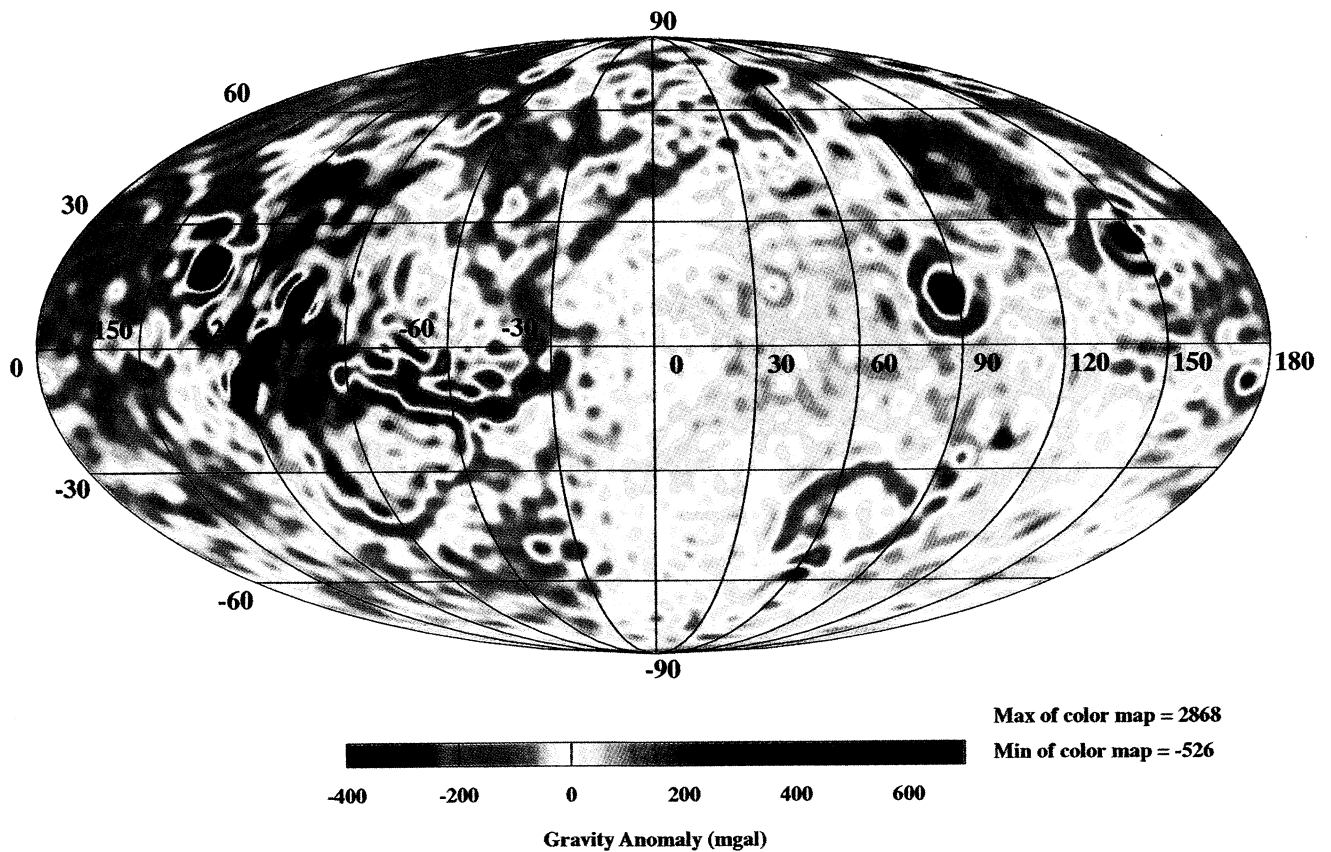


Plate 1. Gravity map derived from MGS observations. Gravity anomaly is computed as the difference of modeled gravity on the areoid and the normal gravity due to a reference ellipsoid on the ellipsoidal surface. Modeled gravity and areoid are computed from 60x60 degree and order terms of the 75x75 MGS75D gravity model. The normal gravity is that of a homogeneous ellipsoid with semimajor axis $a = 3397$ km, inverse of flattening $1/f = 196.87736$, mass $GM = 42828.358 \text{ km}^3 \text{ s}^{-2}$, and rotation rate $\omega = 7.0882181 \times 10^{-5} \text{ rad s}^{-1}$; for the comparison, the J_2 term of the modeled gravity has been reduced to 95 percent of the observed. Projection is equal area Mollweide. Map is consistent with earlier versions while showing considerably increased detail. One milligal (mgal) is $10 \mu\text{m s}^{-2}$.

This illustrates the manner in which the variations in geometry affect the occultation points. Notice that the opening and closing of the loops, i.e., the start and end of occultation periods, are marked by rapid variations in occultation latitude that are of the order of 1 deg/d. Typically, the occultations begin and end at midlatitudes with the ingress and egress points drawing away from or moving toward the equator. This rapid N-S variation in the location of the occultation points has proved useful for probing the meridional structure of the atmosphere [Hinson *et al.*, 1999]. Most of the interval within an occultation "season," however, finds the latitude of occultations confined to a fairly narrow range in the polar regions of Mars. These periods are useful for studies of zonal variations of the atmospheric structure as the planet rotates $\sim 29^\circ$ beneath the MGS mapping orbit between occultation events at the same latitude [Hinson *et al.*, 2001].

2. Investigation of the Gravity Field

2.1. Overview

Knowledge of Mars' gravity field inferred from systematic observations of the MGS low-altitude polar orbit constrains internal models of the core size and other interior structure at geophysically useful accuracies. The availability of such observations is key to study of the history of the planet. Prior to MGS the best source of information on the gravity was from the Viking Orbiters. Low-altitude measurements from Viking were limited largely to the latitudes of the landers, however, so uniform global coverage was not available. While, for example, the gravity anomaly at Isidis Planitia was known, the gravity over features such as the Hellas Planitia basin, the large volcanoes, and the polar regions had not been measured at high spatial resolution. Similarly, there was very little quantitative information on the thickness of the crust, the strength of the lithosphere, or the variation of these characteristics with position on the planet. For purposes of studying the internal structure, topographic data obtained by MOLA form a critical adjunct to models of the gravity field since the variations in gravity may be employed to constrain internal structure only after the gravitational effects are adjusted for both the global and local shape of Mars.

Spin axis orientations determined from Viking data (1976–1978) and Mars Pathfinder [Folkner, 1997a, 1997b] have provided a good estimate of the pole precession rate and its present orientation. Precise determination of the gravity field by MGS provides an independent estimate of the orientation of the principal axes of inertia and also demonstrates for the first time an ability to sense the spin axis and rotation of Mars at useful levels from orbital data alone. This capability will allow definitive calculations of the moments of inertia without the usual assumptions. Also, the homogeneity factor c/MR^2 (where c is the moment of inertia

along the polar axis, M is the planet mass, and R is the mean radius) can be extracted, allowing one to constrain interior structure models such as core size and radial density variations [Bills, 1989a, 1989b; Kaula *et al.*, 1989; Reasenber, 1977].

2.2. Approach and Methods

Study of Mars' gravity with MGS emphasizes spherical harmonic representation of the field with sufficient degree and order to reveal physically interesting local variations, as well as the global structure. Doppler tracking and range measurements spanning periods of a few orbits to several days yield accurate spacecraft trajectory solutions. Simultaneously with reconstruction of the spacecraft orbit, observation equations are derived for roughly 5800 field coefficients, corresponding to the spherical harmonics through degree and order 75 plus a small number of ancillary parameters, where the size of the solution is chosen to control aliasing and related effects. Currently, such solutions are meaningful through degree and order ~ 62 . Such a comprehensive field solution is essential for characterizing tectonic phenomena such as the Tharsis bulge and is also useful for the study of localized features such as large craters. For example, the gravity solutions evince major uncompensated gravitational anomalies in association with Argyre, Isidis, and Utopia Planitia, and Valles Marineris, as well as anomalies associated with the major volcanoes Olympus Mons, the Tharsis Montes (Ascraeus, Pavonis, and Arsia Mons), and Elysium Mons [Smith *et al.*, 1999a; Zuber *et al.*, 2000].

Prior to MGS the best approach to solution of the gravity field was not clear. It was known that gravitational anomalies on Mars are substantially larger in both a relative and an absolute sense than those of Earth. That these could be sensed and characterized by use of line-of-sight tracking measurements was well established [Sjogren, 1979], but the best method for construction of representative models was a matter of some debate. Previously, in planetary work with spacecraft, large anomalies were often modeled as discrete features whose physical characteristics were obtained by fitting simulated effects to the line-of-sight data. Low degree and order spherical harmonic solutions based on classical methods and data from Mariner and Viking appeared to work well, as they do for Earth, but large errors occurred when these models were used to predict spacecraft motions at low altitudes. The degree and order 18 spherical harmonic solution described by Balmino *et al.* [1982] represents the Viking era standard for geophysical studies of Mars.

Application of both line-of-sight and spherical harmonic methods was planned in the Mars Observer era. For either approach, simple physical arguments utilizing preflight estimates of MGS tracking performance indicated that more than an order-of-magnitude improvement in accuracy over previous field models could be

expected, with uniform global coverage resulting from the choice of the MGS orbit. Reanalyses of Viking and Mariner data, taking advantage of the considerable increases in computational resources since 1982, were used by the gravity investigators to develop methods for much larger solution fields, and to improve the initial fields in support of MGS navigation during the aerobraking phase. *Smith et al.* [1993], *Konopliv and Sjogren* [1995], and *Smith et al.* [1995] were successful in correcting problems in previous large expansion field solutions and demonstrated that the spherical harmonic approach was feasible to high degree and order. This approach was adopted by the gravity investigators and has been applied extensively to obtain MGS solutions.

The low, 170-km periapsis altitude of the MGS SPO provided a unique opportunity to exploit the line-of-sight technique. A total of 93 line-of-sight profiles were obtained in SPO-1 and SPO-2. These provide the strongest and highest-resolution information available on Mars' gravity along the surface tracks.

Preliminary MGS radio science solutions for the gravity field from both Goddard Space Flight Center (GSFC) and the Jet Propulsion Laboratory (JPL) are described by *Smith et al.* [1999a]. The results are in the form of spherical harmonic representations of degree and order 70 (GSFC) and 75 (JPL) but presented only to degree and order 48. These fields are based on premapping orbits with periapsis as low as 170 km above the surface of Mars; the nominal surface resolution is ~ 400 km. A more recent solution (MGS75D) of degree and order 75, presented as gravity anomalies to degree and order 62, is presented in Plate 1. Plate 2 provides an enlargement of the area north of Chryse Planitia, illustrating the existence of negative gravity anomalies resembling outflow channels to the north of Valles Marineris; there is no topographic surface expression of these features [*Zuber et al.*, 2000].

To date, the MGS fields have been produced by groups at GSFC and JPL. Although the resulting solutions are very similar, and may be indistinguishable at a geophysical level, the approaches to the solution are different in detail. The convergence of the solutions gives confidence as to their correctness and stability. *Lemoine et al.* [this issue] and *Yuan et al.* [this issue] provide results and discussions of the methods employed.

The quality of the current field is indicated in Figure 3, which displays the power in the harmonics and the associated standard deviation. As can be seen, the standard deviation rises to equal the power for degree $n \approx 62$, at which point the solution error is at or near the level of the result. For lower values of degree the standard deviation decreases rapidly and is negligible relative to power for degree less than ~ 50 , so that any residual errors in the low degree and order coefficients of the gravity field arise from errors in modeling or instability in the solutions. As can be seen, the spectrum of a solution obtained without constraints on the spectral

shape diverges from the systematic downward trend at approximately degree $n \approx 63$ –65, after which it rises with increasing n . This divergence represents an instability in the inversion process that appears roughly at the point where sensitivity to surface detail is lost owing to the finite altitude of the MGS spacecraft. The spectrum of a solution constrained by *Kaula's* [1966] rule, on the other hand, continues to follow a smooth trend with increasing degree to degree $n > 70$, but solutions in the region $n \geq 63$ –65 are not thought to be meaningful [*Lemoine et al.*, this issue; *Yuan et al.*, this issue]. On the other hand, harmonic coefficients below degree and order ~ 35 are determined with considerable certainty, and the low degree zonal harmonics are observed to change with time [*D. E. Smith et al.*, 2000]. More work is required to understand and interpret the time variations, however.

2.3. Global Correlation of Gravity and Topography

The MOLA investigation has now defined the topography of Mars to an extraordinary level [*Smith et al.*, 1999c, this issue]. This has been possible, in part, because of the joint precision orbit reconstruction and the geoid made possible by the radio science study of gravity. Given the MOLA data and assuming a constant crustal density, one can compute the direct gravitational effect of the topography and subtract it from the observed field. The residual Bouguer field is an indication of the degree of isostatic compensation, that is, the degree to which relaxation of strain has progressed toward the condition where there is mass deficiency under the topographic highs and mass excess under the basins, equivalent to "roots" of crustal material in the first case and a thinning of the crust in the second. On the basis of this observation, flexural models have been proposed that describe how the elastic lithosphere bends under the load of the topography, implying a lithospheric thickness variable with the lateral scale or "wavelength" of the surface features [*Turcotte et al.*, 1981; *Balmino et al.*, 1982]. This approach recently has been extended making use of the RS gravity and MOLA topography to obtain a model lithosphere complete through degree and order 60 [*Zuber et al.*, 2000; *Phillips et al.*, 2001].

3. Investigation of the Atmosphere

3.1. Overview

Radio occultations contribute detailed measurements to an improved understanding of the basic thermal structure, circulation, and dynamics of the atmosphere of Mars. These results are based on analysis of the radio signal received from MGS as it enters and exits occultation by the planet. Occultation studies with MGS encompass a range of diverse phenomena (e.g.,

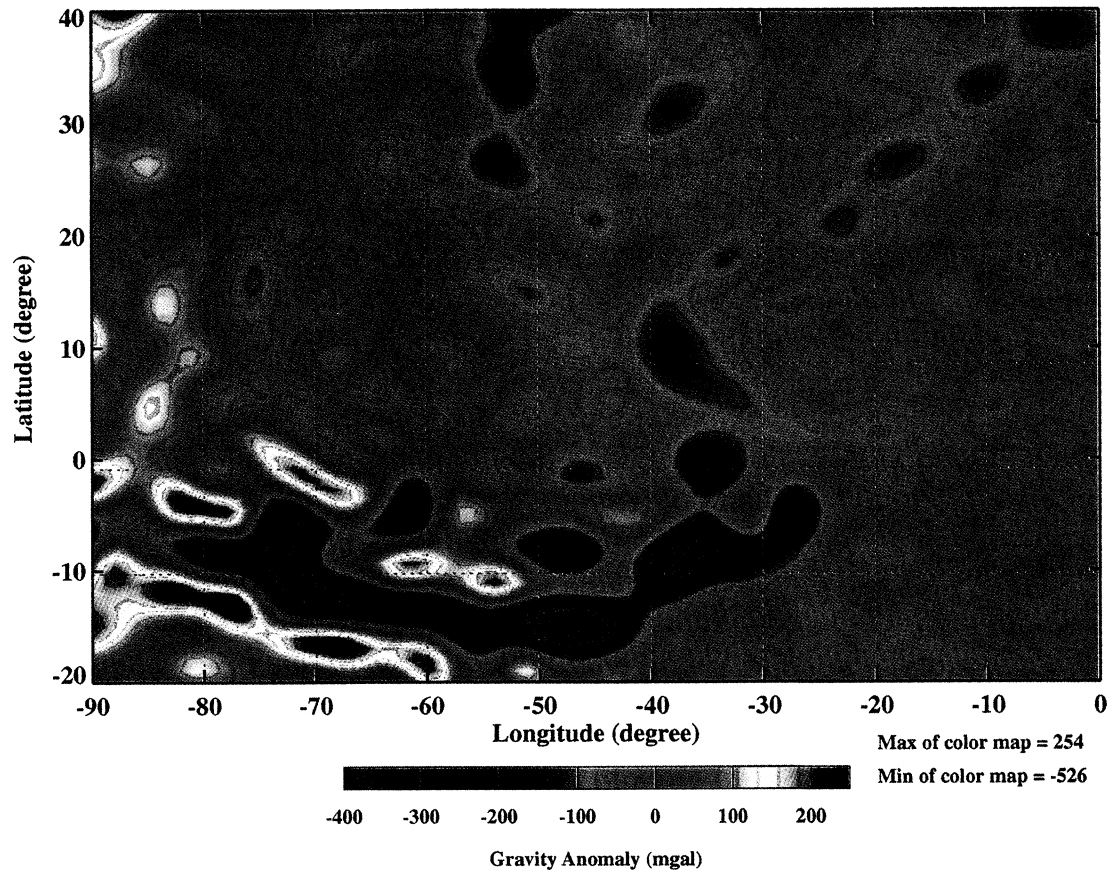


Plate 2. Detail of gravity near Chryse Planitia. Residual accelerations same as Plate 1. Figure shows region of Valles Marineris, Chryse Basin, and southern Acidalia Planitia.

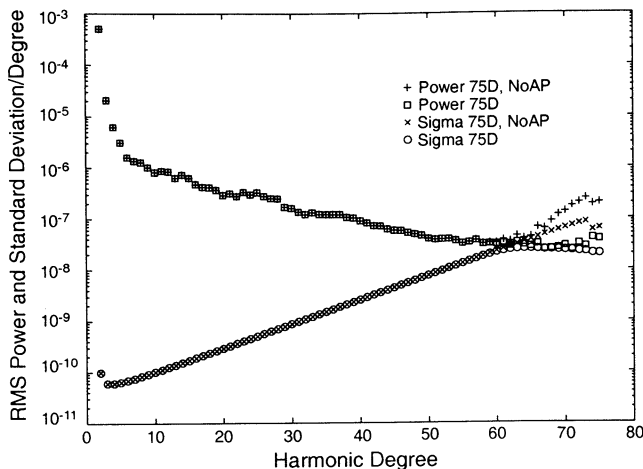


Figure 3. Root-mean-square spherical harmonic power and standard deviation of error versus harmonic degree for two versions of the MGS75D gravity field solution. Figure gives the power in the spherical harmonic coefficients of a given degree, together with an estimate of the standard deviation of the error. “NoAP” indicates no *a priori* constraints applied; alternate solution is constrained by *Kaula’s* [1966] power spectrum. Solutions are essentially the same below degree 62, where power and error come together. Beyond about degree 62 the unconstrained power rises with uncertainty, while the constrained power remains “well-behaved” to at least degree 70 even though error exceeds signal there. Solutions are believed to be reliable below degree ~ 62 on basis of similarity of constrained and unconstrained solutions for lower degree harmonics. Results are typical of MGS determinations of the gravity field to date.

the structure of the planetary boundary layer and the behavior of large-scale eddies and waves) that can be investigated based on high vertical resolution profiles of atmospheric density, pressure, and temperature.

3.2. Approach and Methods

Retrieval of atmospheric profiles requires measurement of small, $\delta f \sim 10^{-3}$ Hz, frequency shifts (or equivalently, phase changes) imposed on the radio signal by the varying refractivity of the atmosphere with height in combination with the motion of the onboard spacecraft transmitter. Extraction of the atmospheric effects from the measurements requires accurate knowledge of the spacecraft trajectory, obtained here as a by-product of the gravity investigations. Standard retrievals yield atmospheric structure, i.e., density, pressure, and temperature versus absolute radius from Mars’ center of mass, to altitudes of ~ 40 km with a vertical resolution in the range 0.5–1 km as set by sampling considerations. The radius of the occultation beam at the surface is estimated to be ~ 100 m, based on the Fresnel-zone size of the radio signal. High-resolution profiles with vertical resolutions as fine as 10–20 m are also planned, based on additional processing in which diffraction effects are removed [Karayel and Hinson, 1997].

3.3. Results for the Neutral Atmosphere

Here we provide two examples of atmospheric results intended to illustrate the quality and the strength of the observations. Figure 4 provides a comparison of the surface pressure as determined from MGS radio occultation with Viking measurements on the surface in 1976–1980. In Figure 4 the stipples forming a continuous curve provide daily average pressures at the Viking 1 landing site (22.3°N , 48.2°W) during late spring through summer, $L_s = 60\text{--}180^\circ$ [e.g., Zurek *et al.*, 1992]. Occultation measurements from three different short time periods appear as asterisks located at $L_s \approx 75^\circ$, 110° , and 140° . The occultation results in the first two groups are from a variety of longitudes, while within each group the latitude is almost constant. The third group comprises occultation measurements from early mapping in the vicinity of the Viking 1 lander (VL1), with separations of 90–1500 km. In order to make the comparison with Viking, the occultation measurements have been interpolated to the same geopotential surface as the Viking 1 lander using an MGS determination of the geoid. In the absence of dynamical atmospheric processes the pressure on such a surface would not vary with position. There is good agreement between the occultation measurements and the lander results, although the two sets of observations are separated in time by 2 decades and by up to 49° in latitude. The largest mean discrep-

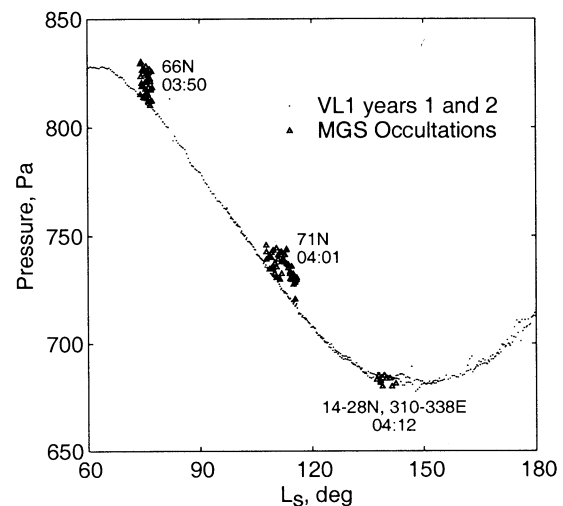


Figure 4. Seasonal variation of atmospheric pressure on a geopotential. Figure compares measurements of Mars’ surface pressure made by Viking 1 lander (1976–1980) and MGS radio occultation (1998–1999). Curve defined by numerous small dots is daily average pressure from Viking 1 [R. J. Wilson, private communication, 1999]; triangles are from MGS radio occultation. Observations are separated by more than twenty years and occur at different locations on Mars. MGS values are interpolated to the same geopotential as Viking 1; in a static atmosphere all values should be the same. Small differences between Viking 1 and MGS observations at high latitudes are believed to result from atmospheric dynamics.

ancy is ~ 10 Pa, or roughly 1.5%, for the points with the greatest latitudinal separation. The agreement is best for $L_s = 140^\circ$, corresponding to occultation measurements made nearest the landing site, where the difference is well under 1%. Considering that dynamical effects in the atmosphere can alter the pressure on a constant geopotential surface, the systematic offset and greater variability of the high-latitude occultation results could be due to dynamic effects. In addition, we are comparing the daily averages from VL1 with the occultation results for early morning near 0400 LT; therefore tidal variations in surface pressure could influence the comparison, although the pressure at 0400 LT is close to the expected daily tidal average. Given these considerations the agreement in Figure 4 is satisfactory.

The comparison above is made possible by an inherent property of the radio occultation measurements that parameterizes the atmospheric structure as a function of radius from Mars' center of mass. That is, the retrieved atmospheric structure is of the form $T(r), p(r)$, or more compactly, $T[p(r)]$, where r is the radius from Mars' center of mass at which temperature T and pressure p obtain. In the MGS implementation, in which the occultation measurements are reduced relative to precision orbits determined by the radio science gravity investigators, the characteristic uncertainty in r is ~ 1 m [Yuan *et al.*, this issue; Lemoine *et al.*, 2000]. Mars' geoid is also known to very high accuracy from integration of the gravity field determined by tracking of MGS.

As an example of the sampling obtained by a typical series of MGS occultations, Figure 5 presents a sequence of 12 occultation profiles near 10°N . These profiles were obtained during a single day of MGS tracking. Similar data sets obtained over several days often provide repeat observations at the same location on Mars. Typically, such repeated measurements are essentially the same, illustrating the considerable control of atmospheric conditions by season, location, and local time of day on Mars, as well as the ability of MGS to obtain meaningful observations of such phenomena [Hinson *et al.*, 2001].

Hinson *et al.* [1999] use the geopotential to organize meridional atmospheric structure observed during the aerobraking phase and to find the gradient zonal winds as a function of latitude. The geopotential also organizes the zonal atmospheric structure, such as that in Figure 5, for study of atmospheric waves in late northern spring, $L_s = 74^\circ\text{--}77^\circ$ [Hinson *et al.*, 2001]. Such an analysis reveals a variety of wave phenomena that are difficult to observe by other than in situ methods, including Rossby and Kelvin waves of various zonal wave numbers. Interpretive use of general circulation models (GCMs) in deciphering various wave phenomena [Hinson *et al.*, 2001; Joshi *et al.*, 2000] is an important aspect of the analysis of these measurements.

3.4. Ionosphere

MGS radio occultation observations sense the ionosphere in addition to the lower layers of neutral gas,

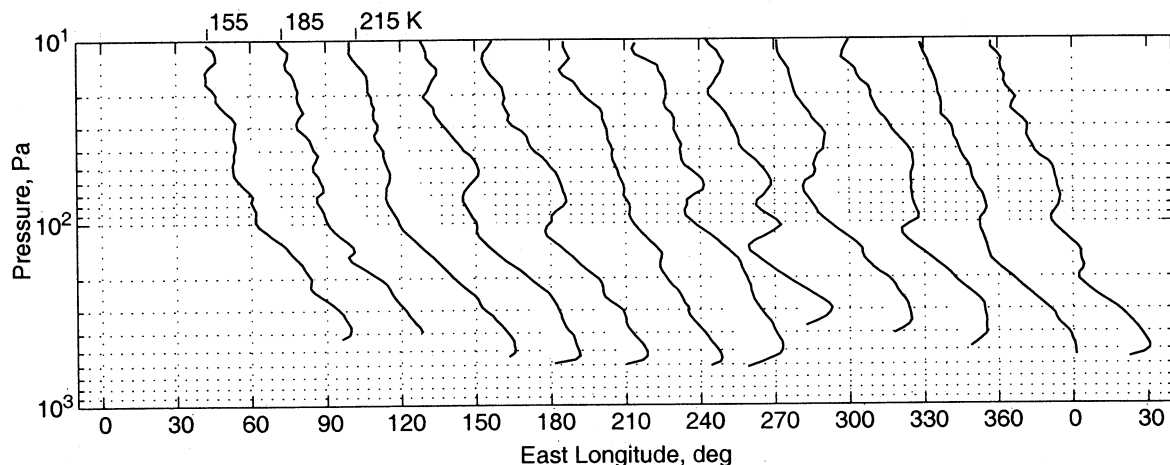


Figure 5. Example ingress occultation soundings at 10.4°N , May 24, 1999. Twelve $T(p)$ profiles acquired during one 24 hour period, are equally spaced in longitude by Mars' constant rate of rotation and the spacecraft's ~ 118 min orbit. Season was mid-summer ($L_s = 144^\circ$) at 0409 local solar time. Longitude of each measurement is given by the location of the topmost point on the curve; e.g., leftmost curve represents data from 42°E . Topside boundary condition for temperature for each curve was taken as 155 K. (Errors in the boundary condition are quickly reduced by measurement constraints at lower altitudes.) The scale of temperature variation is shown above the leftmost profile and has the same index spacing as the longitude. Lowest point on the leftmost profile is 209 K at 431 Pa. Value of the maximum pressure for each curve follows the surface pressure at the occultation point. Of interest here is the variability in atmospheric structure among the curves. Note the early morning temperature inversion near the surface at most locations, as well as the elevated inversions in a number of the profiles, e.g., at 100 Pa on the curve at 241°E . See Hinson *et al.* [2001] for analysis of such a set of curves.

and this is an important aspect of the atmospheric investigation. Owing to use of the 3.6-cm wavelength (X-band) signals, however, the sensitivity to electron content is reduced significantly as compared with earlier Mars observations at wavelengths in the range of 12 cm (S-band). Typical uncertainties in retrieved electron density from MGS are $\sigma_{N_e} \approx 3 \times 10^3 \text{ cm}^{-3}$, as compared with a characteristic peak density of $N_e \approx 80 \times 10^3 \text{ cm}^{-3}$ observed at a solar zenith angle of 80° . In addition, the geometry restricts observations to a region near the terminator where the electron concentrations are already low. Thus, while the ionospheric signal often results in a reliable, well-defined profile, at other times and higher zenith angles the ionosphere is not detected. We anticipate that the dense sampling of the ionosphere in longitude will provide insights into wave structures at high altitudes, in addition to the information constraining models of the photochemistry and high-altitude processes.

4. Other Studies

4.1. Surface of Mars

During occultations by Mars, there are brief periods when radio signals transmitted by the spacecraft incidentally illuminate the planet's surface. The first such echoes were reported during Mariner 6 and 7 flybys by *Fjeldbo et al.* [1972], apparently from specular reflection by smooth, horizontal surface elements near the limb that are mutually visible from both the spacecraft transmitter and Earth receiver. Geometrical and conventional physical optics interpretation methods [e.g., *Fjeldbo*, 1964; *Hagfors*, 1968; *Ogilvy*, 1991] are inadequate because only the smoothest, illuminated (and hence in this instance most elevated) facets can contribute to scattering at the low grazing angles involved. More sophisticated modeling is difficult because of the competing shadowing and diffraction processes [*Beckmann*, 1965; *Sancer*, 1969; *Vesecky et al.*, 1977; *Bass and Fuks*, 1979; *Vesecky et al.*, 1988]. The detection of echoes with significant strength at grazing angles of less than 0.5° suggests that an important fraction of the surface in the scattering areas is smooth on the scales of 1–100 wavelengths.

The great majority of occultations are accompanied by surface echoes. Figure 6a shows signal strength as a function of time and frequency for a typical ingress occultation. The directly propagating carrier signal appears as the extended horizontal line which begins at the left margin near 1300 Hz. The surface echo appears as the diagonal line which begins at ~ 1005 s and merges with the direct signal as the direct signal disappears at ~ 1034 s. Note that the surface echo appears to continue at a frequency lower than the carrier for several seconds beyond the occultation point. This is the result of diffraction of the direct signal into the geometric shadow behind the planet's limb. Figure 6b shows the

power in a 34-Hz bandwidth centered on a straight line fitted to the echo trajectory. Near the time of occultation the power measurement, at "C," is dominated by the direct signal (the amplitude is clipped in Figure 6), but otherwise it is a good measure of the strength of the surface echo. The highly variable echo power between 1009 and 1025 s, at "B," is a common feature of these echoes, and may be related to variations in surface properties or to interference effects among signals reflected from slightly different locations. The sharp cutoff at 1009 s is an artifact of the processing, which abandons the straight line fit near the receiver filter upper cutoff at 2250 Hz, and simply accumulates noise. The experimental geometry, however, typically results in a reduction in the echo strength near this location as the spacecraft antenna radiation pattern illuminates the surface only weakly this early in the occultation event. The weak echo strength in the short interval 1026–1027 s, at "A," is also typical and is probably caused by large-scale shadowing as incidence angles become almost 90° . The strong increase in signal strength at 1030 ± 1 s is not typical, suggesting the presence of an anomalous scattering region very close to the occultation point. We have examined Viking image mosaics in this area, however, and found nothing unusual. The specular point ground track begins near (73°N , 253°W) and ends near (72°N , 252°W).

4.2. Gravitational Radiation

The radio tracking system on MGS was applied during interplanetary cruise to a search for low-frequency gravitational radiation. Gravitational waves (GWs) are propagating, polarized gravitational fields [e.g., *Thorne*, 1987] which can be treated as a propagating strain of space-time. Such waves, which are predicted by all relativistic theories of gravity, change the distance between separated test masses and the rates at which separated clocks keep time. GWs are characterized by dimensionless strain amplitudes, $\delta\ell/\ell$ or $\delta v/c$, where ℓ is the fiducial distance between the masses, δv is their relative velocity, and c is the speed of light. Attempts at direct detection of GWs are intended to verify, bound, or refute a strong-field prediction of relativistic gravity theory. In addition to this important question, if detected, they would offer a new window for observational astronomy.

The DSN tracking system continuously measures the relative dimensionless velocity, $2\delta v/c = \delta f/f_0$, between Earth and MGS. This is currently the only GW observational technique in the so-called low-frequency band (~ 0.0001 – 0.1 Hz). A gravitational wave of strain amplitude h incident on the propagation path causes small perturbations in the tracking record. These perturbations are of order h in $\delta f/f_0$ and each perturbation is replicated three times in the Doppler data [*Estabrook and Wahlquist*, 1975]. As a consequence, a single short gravity wave event is expected to result in three copies

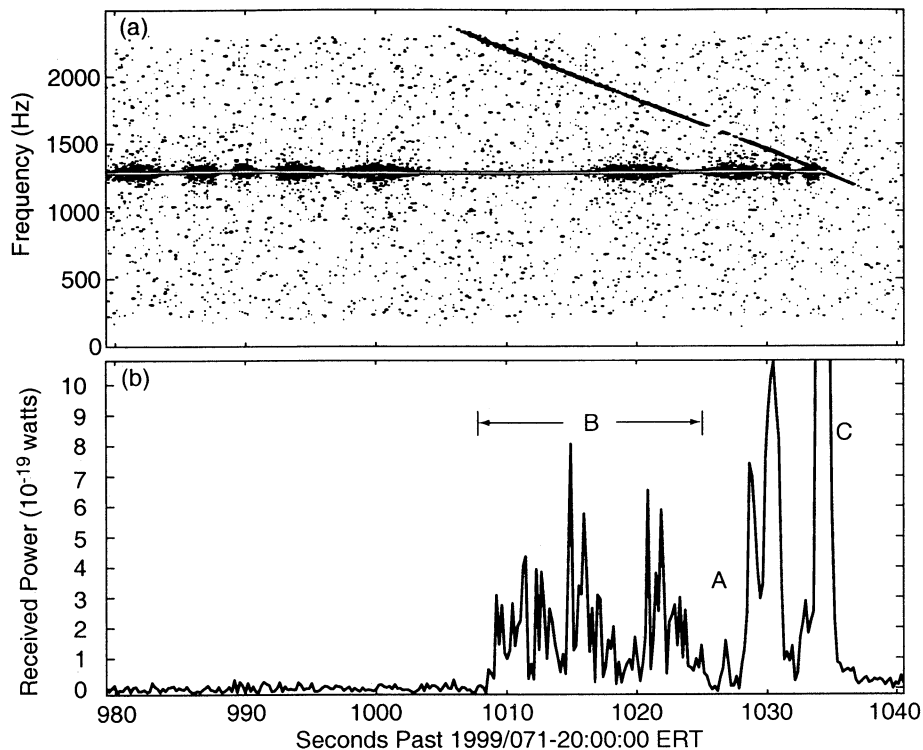


Figure 6. Example of surface scattering observed during occultation. (a) Contour plot of signal strength versus time and frequency for the ingress occultation on MGS mapping orbit 46. The directly propagating carrier signal is represented by the horizontal line at ~ 1300 Hz; carrier signal has been clipped to facilitate display of the surface echo, which appears at ~ 1005 s and moves diagonally to merge with the carrier at the occultation point (1034 s). Scalping around the carrier is a processing artifact as the carrier frequency drifts slightly with respect to frequency analysis bins. The spacecraft antenna first illuminates the surface a few seconds before the echo moves into the receiver passband. (b) Total power in 34 Hz centered on a linear fit to the echo trajectory.

of itself in the Doppler data stream. The sum of the total Doppler perturbations, three time-spaced signals in the observational data, is zero. Gravity wave disturbances with durations longer than approximately the one-way light time (OWLT) produce overlapping responses in the tracking record in such a way that the net response cancels to first order. The tracking system thus has a band pass response to gravitational excitation. The low-frequency band edge is set by the cancellation effect to be roughly OWLT^{-1} , while thermal and other noise sources in the radio system limit the observable high-frequency response to ~ 0.1 Hz. The sensitivity within this passband is determined primarily by competition of the GW signals with propagation noise arising from solar plasma and tropospheric scintillation.

High-quality Doppler data were obtained while MGS was in quiet interplanetary cruise between the Earth and Mars, from April 14 to May 4, 1997, when the Sun-Earth-spacecraft angle was $\sim 125^\circ$. These MGS X-band data are roughly an order of magnitude more sensitive than previous generation S-band (2.1 GHz uplink and 2.3 GHz downlink) observations and are the most sensitive to date in the low-frequency band. The high-

quality results from use of X-band radio technology, which strongly suppresses plasma scintillation noise, and from the favorable Sun-Earth-spacecraft geometry. Some MGS noise statistics and their application to GW searches have been presented by *Armstrong* [1998] and *Tinto and Armstrong* [1998]. The noise level of the MGS system, expressed as $2\sigma_{\delta f/f}$ in the $\sim 6 \times 10^{-7}$ Hz resolution bandwidth of the observations, is less than $\sim 10^{-15}$, where $\sigma_{\delta f/f}$ is the standard deviation of the two-sided spectrum. Coupling of GWs to the Doppler observable depends on the angle between the direction to the source and the Earth-spacecraft line. Unlike most other missions, MGS had an excellent geometric transfer function for the direction to the galactic center, the nearest plausible sources of strong GWs. Analysis is ongoing for periodic, impulsive, and stochastic GWs. The MGS sensitivity will not be bettered until the Cassini GW experiment planned for 2002–2004. The Cassini radio system is designed to extend observations to lower frequencies with a sensitivity expected to be roughly an order of magnitude better than that demonstrated with MGS. Nevertheless, MGS has demonstrated improvements in the design and implementation of spacecraft GW detectors. Further, the close scrutiny applied to

the Doppler system performance as part of the GW investigation has been beneficial to the classical gravity and occultation investigations of Mars.

5. Radio Science Experiment Design

5.1. Routine Observations

Radio science observations are highly constrained by viewing geometry and DSN tracking coverage. In the case of gravity observations a ground station must be actively transmitting and receiving while the spacecraft is visible from Earth. Although the spacecraft is in a nominal 7-day repeat orbit [Albee *et al.*, this issue], complete coverage of the planet's gravity field takes much longer owing to the noncontinuous nature of the DSN tracking schedule.

The nominal observing schedule for MGS includes one DSN pass (~10 hours) per day with an additional pass every third day. Each 10 hour pass corresponds to about five MGS orbits yielding five ingress and five egress occultations and about five 80-min "arcs" of tracking data.

Two distinct types of radio science observations are carried out during each pass: (1) "open-loop" measurements of atmospheric occultations and (2) "closed-loop" tracking measurements of the gravity field. Each occultation observation includes (1) the interval during which the spacecraft-to-Earth ray path passes within 200 km of the surface, (2) an additional period of 20 s in geometric occultation by the solid body of Mars, (3) a baseline interval of 100 s during which the proximate point of the ray path is above 200 km altitude, and (4) an appropriate time interval prior to and following these events to protect against timing errors in the spacecraft trajectory predictions. Gravity field observations are implemented by collection of tracking data during the remainder of the orbit while the spacecraft is visible from Earth.

5.2. Anomalies

Difficulties in the articulation system for the high gain antenna (HGA) [Albee *et al.*, this issue] prevent pointing the radio beam continuously toward Earth throughout a complete MGS orbit during those periods when the direction to Earth is less than about $+43^\circ$ from the orbit plane. As a consequence, maintenance of the nadir pointing spacecraft attitude results in a loss of the occultation emersion, i.e., the southernmost, observations. This loss is mitigated by a special sequence that provides one or two 24 hour periods each month during which the operation of other instruments is interrupted to provide occultation sampling of the atmosphere during occultation emersion. In the nominal sequence the HGA articulation system "unwinds" while the spacecraft is in Earth occultation. The HGA articulation problem has forced the unwind procedure

into the period when MGS is on the Earth side of Mars during affected orbits with the result that ~10 min of tracking data are lost from each Earth-side pass.

5.3. Coordinated Observations

Mars Observer plans included coordinated observations of the atmosphere by the radio science (RS), pressure modulator infrared radiometer (PMIRR), and thermal emission spectrometer (TES) instruments [Tyler *et al.*, 1992]. Following the loss of Mars Observer and definition of the MGS experiment complement, similar coordinated observations were planned for RS and TES, and it was hoped that inter-project observations might be possible with PMIRR on Mars Climate Orbiter (MCO). With the loss of MCO joint investigations were limited to RS and TES and conducted during a 10 day period in December 2000.

The purpose of the joint RS-TES observations is to compare results from observations of the same parcel of atmosphere obtained by infrared limb sounding with TES and by radio occultation. Such a comparison, which has not been attempted before, is expected to be highly informative as centimeter-wavelength radio signals are insensitive to the presence or absence of atmospheric aerosols (dust and clouds) *per se*, while the IR results from TES are strongly coupled to aerosols [Conrath *et al.*, 2000; M. D. Smith *et al.*, 2000], and because the inversion methods are disparate. Methodological questions of interest include the effects of the distinct inversion kernels on retrieved atmospheric profiles such as the importance of dust and atmospheric variability, possible detection of systematic differences between the two methods, and the effects of sampling volume. Atmospheric questions that may be addressed by such joint investigations include the lateral and vertical scale(s) of atmospheric variability, the opacity, and processes in the gas volume actually sampled, such as condensation.

This observation is properly carried out at times when Earth passes through the MGS orbit plane. During normal operations, TES can carry out vertical limb scans in the orbit plane; radio occultations, however, occur along the path defined by the spacecraft-to-Earth line. When Earth passes through the orbit plane, both instruments can view simultaneously the same volume of atmospheric gas.

The joint TES-RS observations are one example from a set of coordinated and particularized observations known as "campaigns." Additional campaigns involving atmospheric RS are designed, for example, to characterize seasonal differences (especially at the poles), to exploit the enhanced signal-to-noise ratio (SNR) obtained at opposition, and to take advantage of rapid changes in occultation latitude. Gravity results are improved by campaigns selected for maximum SNR and increased observational intervals at the solstices.

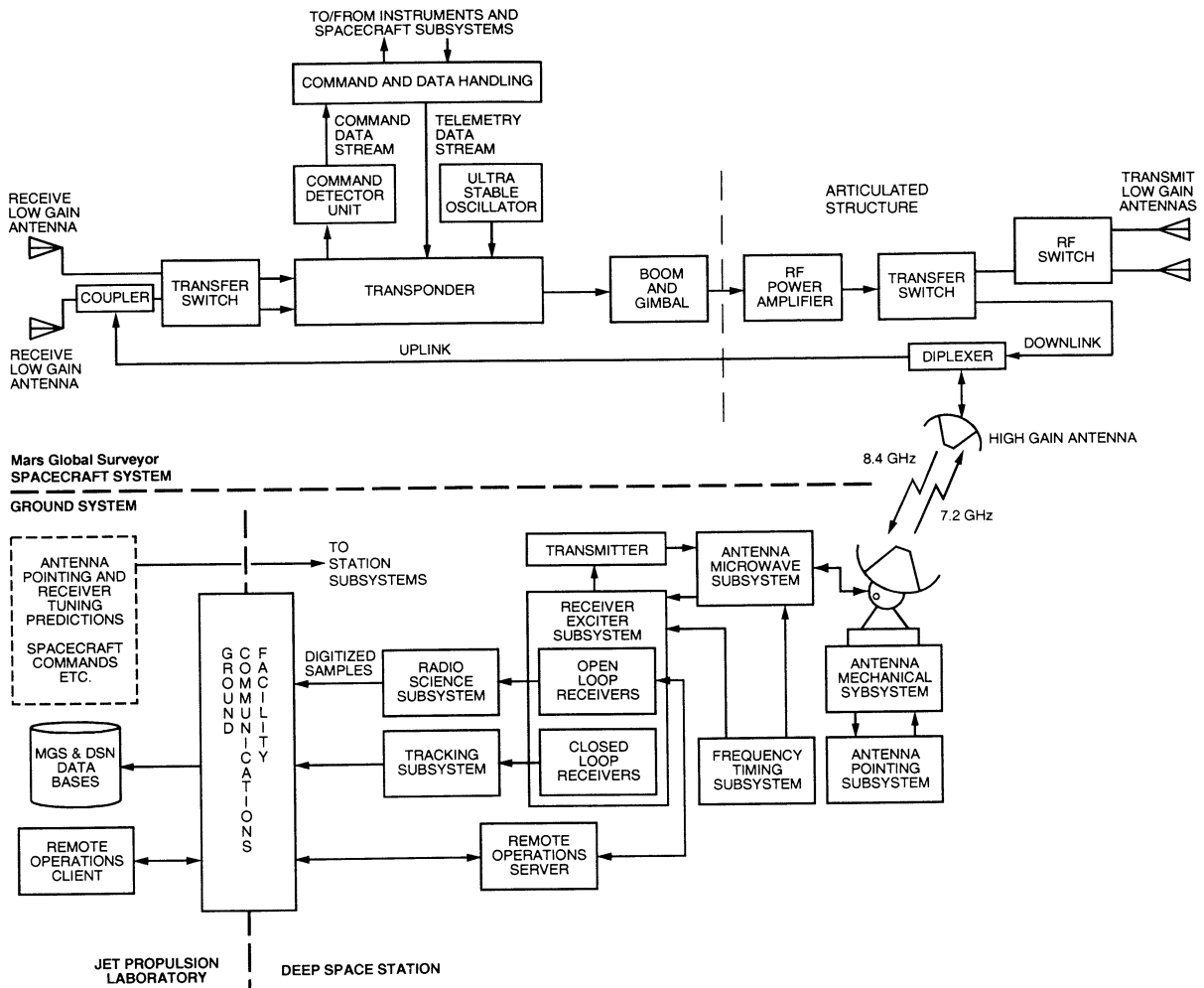


Figure 7. Elements of Mars Global Surveyor spacecraft and NASA Deep Space Network radio and tracking system. Instrument comprises spacecraft and ground elements, shown in the upper and lower sections of figure. Spacecraft transponder and high-gain antenna are used for both atmospheric and gravity investigations. Spacecraft antenna assembly to right of “Boom and Gimbal” are on articulated structure. HGA pointing is constantly adjusted to maintain fixed direction to Earth as spacecraft body rotates with position in Mars orbit. Ground equipment is standard to DSN except for “Remote Operations” Client and Server which were put in place to provide partial automation of MGS RS occultation measurements. Radio Science Systems Group at JPL is able to preprogram and monitor operation of the Open-Loop Receivers at DSN stations.

6. Radio Science Systems

The MGS radio science investigations utilize instrumentation with elements on the spacecraft and at the DSN on the ground (Figure 7). Much of this is shared equipment, being used for routine engineering command and telecommunications as well as for radio science. The performance and calibration of both the spacecraft and tracking stations directly affect the radio science data accuracy, and they play a major role in determining the quality of the results. One responsibility of the Radio Science Team has been to help define the equipment configuration and performance and to monitor the operation of these systems.

6.1. Spacecraft Radio System

The spacecraft radio system is constructed around a redundant pair of radio transponders (MOTs), which receive uplink signals from the ground at a frequency of 7.2 GHz and transmit at 8.4 GHz, both of which are “X-band” frequencies. Only a single MOT is shown in Figure 7. The transponder provides the usual uplink command and downlink data transmission capabilities, which we will not elaborate here. The MOT also includes a modulation ranging channel which can be driven either by signals from the ground for measurement of absolute range or by discrete tones generated onboard to enable measurement of differential range be-

Table 2. Selected Characteristics of the Mars Global Surveyor Radio System

<i>Receiving Parameters</i>	
Nominal frequency	7164.6 MHz
Peak antenna gain	37.4 dBi
System noise temperature	540 K
Polarization	right-circular ^a
Carrier tracking bandwidth ^b	18.0±4.5 Hz
<i>Transmitting Parameters</i>	
Carrier frequency:	
USO mode ^c	8423.2 MHz
Coherent mode ^d	8417.7 MHz
Transponder turn-around ratio ^e	880/749
Radiated power, HGA	43.3 dBm
Peak antenna gain ^f	39.1 dBi
Polarization	right-circular

^aLeft-hand helical in space.

^bLoop noise threshold value.

^cOne-way transmission, referenced to USO. See Figure 8.

^dTwo-way tracking. See text.

^eRatio of spacecraft radiated frequency to that received from ground.

^fDiffering microwave system losses are incorporated in the values of transmitting and receiving antenna gain.

tween two ground stations. Selected system parameters are shown in Table 2.

The strength of the spacecraft carrier signal, and thus the quality of the radio occultation data, depend on its modulation state. Telemetry data are encoded and then used to modulate a 1 MHz square wave subcarrier which, in turn, modulates the X-band carrier. Telemetry modulation typically results in carrier suppression of either 15.2 dB during simultaneous transmission of science and engineering telemetry or 9.3 dB during transmission of engineering telemetry only. The two-way ranging channel, when activated, suppresses the carrier by ~0.2 dB; when in use, differential range modulation also suppresses the carrier roughly 0.2 dB. Each modulation type (telemetry, range, and differential range) can be activated independently. Radio occultation measurements are conducted with all modulation suppressed in order to avoid these losses and maximize the power in the downlink carrier. Traveling wave tube amplifiers, driven at saturation, amplify the MOT output before the signals are radiated via a steerable 1.5 m diameter parabolic high gain antenna (HGA). Effective isotropic radiated power is ~82 dBm.

Each MOT generates a downlink signal in either a “coherent” or a “noncoherent” mode, where the transmitted frequency is controlled either by the uplink signal received from a ground station or by an onboard oscillator, respectively. When operating in the coherent

mode the MOT behaves as a conventional transponder; the “turn-around” ratio of transmitted to received signal frequencies is exactly 880/749. The use of a rational value for the ratio of the two frequencies permits a precise comparison of the downlink and uplink signals at the ground station since the inverse ratio can be applied to the received downlink signal, thus enabling direct observation of the round-trip Doppler shift. In the noncoherent mode the downlink carrier frequency is derived from one of the spacecraft’s onboard oscillators independently of the presence of the uplink signal. In this instance drifts between the source oscillator onboard and a reference standard on the ground become a limiting factor in the accuracy of the measurement.

One of the onboard oscillators, the Ultra-Stable Oscillator (USO), has been provided specifically to serve as a precision frequency reference for radio occultation experiments. Designed and fabricated at the Applied Physics Laboratory of Johns Hopkins University, the USO has been positioned within the spacecraft in a manner that minimizes exposure to thermal variations and mechanical vibration. The USO consists of a quartz crystal resonator contained in a temperature-controlled titanium dewar. Its output frequency is ~19.14 MHz. The X-band carrier for noncoherent downlink transmission is produced by multiplying the USO output frequency by 440. The MGS USO is of a newer generation than those flown on the Voyager and Galileo spacecraft. Its frequency stability, as characterized by the fractional Allan [1966] deviation and after accounting for linear drift, is measured to be better than 2×10^{-13} for integration times in the range 1 to 1000 s. This represents more than an order of magnitude improvement in per-

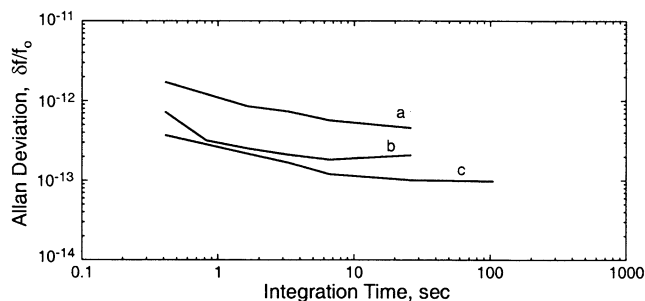


Figure 8. Allan deviation of occultation signals. Three curves show the variation in frequency stability of the MGS-to-Earth propagation path with distance from Earth. (a) 2.5 AU, near maximum Earth-Mars range, MGS in orbit insertion configuration. (b) 0.6 AU, near minimum Earth-Mars range, MGS in mapping orbit. (c) 0.2 AU, in cruise to Mars. Curves indicate characteristic values of the stability. Day-to-day variation at minimum range can exceed the spread in curves shown. Causes of instability are not well understood but include changes in equipment configurations at ground stations, variations in the propagation path, and effects of spacecraft activities on attitude stability.

formance over similar type devices carried by Voyager and Galileo. The overall system level of performance also depends on transmission effects, most importantly on SNR at the ground receiver and the effects of solar wind plasma along the propagation path. Low values of SNR and increased integrated solar plasma both reduce the effective system frequency stability. This behavior is illustrated by the observed Allan deviation under differing conditions in Figure 8. At present the MGS USO has a fractional frequency aging rate of $2 \times 10^{-12}/\text{d}$ while its long term fractional change in frequency after five years is less than 1×10^{-8} .

In contrast with past practice for planetary missions, the HGA is mounted at the end of a 2 m boom, with the result that the phase center of the antenna is on average about 3 m from the spacecraft center of mass. The actual offset between the antenna center of phase and the spacecraft center of mass varies with the articulation of the antenna and the solar panels and with use of fuel. MGS is the first planetary mission (excluding Mars Observer) to operate with such a boom for radio science observations. Since radio tracking and occultation measurements are referenced to the antenna center of phase, while the orbit is referenced to the spacecraft center of mass, the difference must be corrected if meaningful results are to be obtained at the level of accuracy inherent in the radio system. An area of concern to MGS RS and to project navigators is the "pseudo-Doppler" effect introduced into the radio tracking and occultation data by motion of the HGA relative to the spacecraft center of mass and which must be removed during data reduction. Six sources of HGA motion have been identified: (1) the spacecraft rotation needed to maintain nadir pointing while in orbit, (2) articulation of the HGA to maintain Earth point, (3) HGA boom flexure, (4) short term migration of the spacecraft center of mass associated with effects such as "sloshing" of propellants and motions of articulating booms, (5) spacecraft attitude instability, and (6) vibrations at frequencies of a few hertz introduced by the HGA and solar panel stepper motors. The first two error sources are sufficiently deterministic to allow correction by use of rather straightforward modeling. Boom flexure and mass migration are believed to be insignificant on the basis of design and flight tests. Nevertheless, we are unable to correct the antenna boom motion to levels of precision required to preserve the effective stability of a "boomless" system. Operational experience with the boom extended shows that use of this configuration typically increases the Allan deviation over that observed before boom deployment, but the amount of this increase is difficult to characterize. Item (5) remains a concern, but less so than before flight experience was available.

Item (6) was appreciated only after HGA deployment, and it remains a problem. Approximately 5 Hz modulations of the spacecraft carrier have been visible in occultation data collected with SNR higher than

~ 50 dB since mapping operations began with the deployed HGA in early April 1999. The 5 Hz modulation sidebands are excised during standard occultation data processing, but the same may not be true when wider bandwidths are required for high-resolution processing. The ~ 5 Hz modulation is aliased into the more slowly sampled (1 or 10 s^{-1}) tracking data where it represents a serious limitation in use of these data in raw form. The nonrandom nature of these signals means they are not removed by averaging even though the characteristic time scale for gravity variations sensed at 400 km altitude is more than 10 s. Test results suggest that stepper motors for the solar panel array do not affect radio system performance although they have a major effect on TES operations [Albee *et al.*, this issue].

6.2. Ground Stations

Ground stations include antennas, associated electronics, and operational systems in the three complexes comprising NASA's Deep Space Network. In the mapping orbit a nominal 10 hours of daily tracking is obtained using a 34-m diameter "high-efficiency" (HEF) or "beam-waveguide" (BWG) antenna. Science campaigns provide for increased observations during limited intervals [Albee *et al.*, this issue]. Larger antennas (70 m) are utilized occasionally for higher downlink data rates. Measurements of spacecraft range and Doppler can be obtained whenever the spacecraft is visible and a 34-m antenna is available; the 70-m antennas are not equipped with X-band uplink equipment, so acquisition of two-way tracking data to support the gravity investigation requires support by a 34-m antenna for transmitting. Radio occultations can be recorded whenever the spacecraft is visible using either a 34- or 70-m aperture alone. Data from the DSN Monitor and Control Subsystem are analyzed by DSN operational personnel, Radio Science Systems Group personnel at JPL, and the investigation group at Stanford University to monitor the ground instrument operations and health. Relevant parameters describing DSN performance are listed in Table 3.

Once the radio signal from the spacecraft is captured by the ground antenna, it is amplified by a low-noise device. Two measurement options are then available. Open-loop data acquisition is performed by narrowband filtering, typically with a bandwidth of 2.5 kHz, and then downconverting the received carrier signal to baseband where it is sampled for subsequent manipulation in digital form. The open-loop receiver is tuned on the basis of frequency predictions that take into account the best estimate of the carrier frequency transmitted by the spacecraft and Doppler corrections based on relative spacecraft-to-ground motion. These open-loop samples constitute the principal observable for radio occultation. Because only perturbations to the one-way frequency are of interest in determining the properties of the atmosphere, the Allan deviations shown in Figure 8 are

Table 3. Selected Characteristics of Deep Space Network Tracking Stations for Mars Global Surveyor^a

	Value	
	34-m, High-Efficiency Station	70-m Station
<i>Receiving Parameters</i>		
Nominal frequency (from MGS) ^b	8417.7 MHz	8423.2 MHz
Antenna gain	68.1 dBi	74 dBi
System noise temperature ^c	30 K	21 K
Polarization ^d	right or left	right and/or left
Carrier tracking loop threshold bandwidth ^c	10 Hz	10 Hz
<i>Transmitting Parameters</i>		
Nominal frequency (for MGS)	7164.6 MHz	not available
Transmitter power	0.1–20 kW	
Antenna gain	67 dBi	
Polarization ^d	right or left	

^aSince only the 34-m station antennas have an X-band transmission capability, parameters for the 34-m stations are for duplexed operation, and parameters for the 70-m stations are for “receive-only” configuration. The great majority of operations are carried out with the 34-m High Efficiency (HEF) station shown. A third, “Beam Waveguide” station type, with performance similar to 34-m HEF, is used occasionally. The 70-m stations are used infrequently by MGS, but their superior receiving performance is important for some observations.

^bTwo-way downlink, 34 m; one-way downlink 70 m.

^cTypical at zenith.

^dCircular.

^eTypical.

representative of the measurement accuracy under the conditions shown.

Closed-loop data acquisition is performed with a phase-locked loop receiver; it is usually employed when the spacecraft is operating in its “coherent” mode, but also has been used to acquire one-way data referenced to the USO for gravity solutions. Round-trip, “two-way” Doppler shifts are determined by comparing each measurement of the downlink carrier frequency from the phase-locked loop with a reference from the ground station’s frequency and timing subsystem. This measurement of the round trip Doppler shift constitutes the principal observable employed by the MGS Navigation Team and RS gravity investigators. Since the station frequency reference is also used to generate the uplink carrier, the determination can be as accurate as the fundamental station clock, typically, a hydrogen maser frequency standard, which is more stable than the USO. The Doppler integration time needed to achieve a particular SNR controls the time interval between successive measurements. Amplitude of the received signal is estimated by sampling the calibrated automatic gain control (AGC) voltage of the phase-locked loop. One-way closed-loop Doppler shifts are determined in much the same way except that the downlink measurement from the phase locked loop must be compared with an independent estimate of the spacecraft carrier frequency; in this case the accuracy is limited by the performance of the reference oscillator on the spacecraft.

The Doppler errors for one- and two-way tracking are comparable, but are influenced by the effects of

the solar wind crossing the propagation path. Levels of Doppler measurement noise for 10 s integration of the line-of-sight spacecraft velocity are characteristically $10 \mu\text{m s}^{-1}$ at minimum Earth-Mars range ($\approx 0.6 \text{ AU}$), $25 \mu\text{m s}^{-1}$ at nominal range ($\approx 1.5 \text{ AU}$), and $800 \mu\text{m s}^{-1}$ near solar conjunction ($\approx 2.5 \text{ AU}$). Performance improves with decreasing range owing to the combination of increasing signal strength and decreasing path variations from solar wind effects. The best tracking data performance observed to date is $\sim 5 \mu\text{m s}^{-1}$ with Mars near opposition.

7. Data Products

7.1. Overview

Data products from the radio science investigation fall into two broad categories: (1) raw and (2) reduced data. Both are being produced and stored on compact-disc recordable (CD-R) media for the Planetary Data System (PDS). The raw data CD series is subdivided according to mission phases into Cruise, Orbit Insertion, Mapping, and Extended Mission data sets; reduced data CDs are produced only as a single set of Science Data Products.

7.2. Raw Data

The raw data suite comprises both primary and ancillary data. Primary data include the fundamental measurements from the RS instrument: (1) the observed Doppler frequency shift of the received radio sig-

nal, (2) round-trip time-of-flight or range to the spacecraft, and (3) 5 kHz samples of open-loop receiver output during occultations. These products are generated at the ground stations of the DSN. Doppler and range measurements appear in Archival Tracking Data Files (TDFs). The Orbit Data File (ODF) is a derivative of the TDF. ODFs usually form the actual input to solutions for the gravity field; here we define ODFs as “secondary data.” Occultation receiver output samples are captured in Original Data Records (ODRs) from the Deep Space Communications Complex Digital Spectrum Processing (DSP) subsystem.

Ancillary data files contain (1) basic information for interpretation of the raw data, (2) information on important perturbations to the spacecraft or ground system, and (3) calibrations of the propagation path needed for the best accuracy. Such files, for example, describe the orientations of the spacecraft bus, the solar array panels, and the high-gain antenna or, in another instance, they provide weather observations at DSN stations and media calibration files for the Earth’s troposphere and ionosphere. (See Appendix A and tables therein.)

7.3. Reduced Data

The collection of reduced data includes (1) “standard” and (2) “special” products. Standard products are generated routinely once the necessary raw and ancillary files are in hand. These are produced for both the gravity and radio occultation components of the RS investigation. Special products are reduced products that either were not foreseen early in the mission or contain results from secondary investigations.

7.3.1. Atmosphere. Data products from radio occultation studies of the atmosphere include profiles of density, pressure, and temperature versus radius in the neutral atmosphere at standard, i.e., ray optics resolution. Diffraction-corrected profiles at finer than Fresnel zone resolution are planned. Also produced are time histories of the surface pressure and measures of surface radius at the occultation points. Vertical profiles of electron density in the ionosphere are produced from the occultation observations when the ionosphere can be detected.

Standard products from radio occultations include radio occultation temperature-pressure profiles (RSTP) and summary files of occultation results (OCCSUM) containing surface conditions extracted from each atmospheric profile. A radio science intensity power spectrum (RSIPS) file was defined early in the mission, but no unambiguous evidence for scintillations has been discovered and no RSIPS files have been generated.

7.3.2. Gravity. Team investigators have produced several global spherical harmonic solutions, complete to degree and order of 50 to 75, and corresponding covariance matrices of the coefficients. The Mars’ geoid, the gravity anomaly field, and their associated uncertainties

are also obtained. The line-of-sight method produces profiles of acceleration, and contoured maps of reduced gravity disturbances from such profiles were planned originally. Advances in the production of spherical harmonic solutions have resulted in a reduced emphasis on the line-of-sight products; we note, however, the very high quality line-of-sight observations of the north polar region. Additional results, such as mass estimates of near surface structures and power and error spectra are expected over time, but these are not formal MGS products.

Reduced data files from the gravity investigations include spherical harmonic models in both ASCII (SHA) and binary (SHB) formats. The latter include covariance matrices for the spherical harmonic coefficients, which increase their volume substantially. The gravity results are also rendered in map formats giving “free air” gravity and geoid height. These latter products are collectively known as Radio Science Digital Map Products (RSDMAPs). A Line-of-Sight Acceleration Profile Data Record (LOSAPDR) was defined early in the mission but has been produced only for the 93 SPO orbits with 170 km altitude periapsis near the North Pole.

7.3.3. Combined gravity and topography.

Global representation of the topographic heights and global gravitational potential in spherical harmonic expansion will form the basis of several basic map types. Bouguer gravity anomalies, isostatic anomalies, and the admittance function and correlation coefficients between gravity and topography will be obtained. Fundamental properties of the Martian lithosphere will be derived from the basic map types.

7.3.4. Special products. The surface reflection investigation has yielded special products. These include “images” showing the distribution of surface reflections in time and frequency (SRI, see Figure 6), tabulations of surface reflection frequencies and amplitudes (SRT), and summaries of the geometric observing conditions during observation of surface echoes (SRG). About 75 electron density standard resolution (EDS) ionospheric profiles have also been generated as special products.

7.4. Data Availability

Raw and ancillary data, standard data products, and special data products are available from the Planetary Data System (PDS). Appendix A provides a summary of the data file types, acronyms, and numbers of files by mission phase as of January 2001. Delivery of data to the PDS lags data acquisition by about six months to allow generation and validation of both the raw and reduced products.

The Radio Science Team maintains a web site with example results and information of general interest to the public and educators. This site also contains a database with released atmospheric products. The URL is <http://radioscience.stanford.edu/projects/mgs/>.

8. Conclusions

Radio tracking of MGS in combination with its low polar orbit about Mars has led to very strong spherical harmonic solutions for the free air gravity field accurate through degree and order ~ 62 . Owing to limitations of orbital altitude, the current field solution is not expected to change greatly with the inclusion of additional data. That is, the spherical harmonic solution will not be extended much beyond the present degree and order. Temporal changes in the low-degree zonal field have been detected, although more work is needed for interpretation in this area. These changes could reflect phenomena such as changes in the length of day, mass transfer between the polar caps and between the polar caps and the atmosphere, precession of the spin axis, and perhaps internal activity.

Combination of the Martian gravity field from the RS investigation with surface topography from the MOLA investigation allows removal of the effects of local surface shape from the gravity, thereby yielding a more accurate view of the structural variations within Mars.

The result is an extremely powerful constraint on the interpretation of the interior structure and history of Mars [Smith *et al.*, 1999a]. Preliminary models of the planet's interior have been produced by Zuber *et al.* [2000], Phillips *et al.* [2001], and Yuan *et al.* [this issue], giving evidence or interpretation of the age relationships among major structural features, such as the Southern Highlands, Northern Plains, Tharsis Montes, and the hemispherical "dichotomy."

Although observations from previous missions have been included in the most recent MGS solutions, the quality and quantity of the MGS tracking data overwhelms the contribution of the older measurements; only low-periapsis Viking Orbiter data have a discernible effect, and then only at degrees higher than ~ 50 . The lengthening time base of observations, including lander data, continues to be valuable in determining precession of the rotation axis and variations in the length of day, and indirectly, knowledge of the deep interior.

Radio occultation measurements with MGS provide systematic sampling of the neutral atmosphere from the

Table A1. Raw Data Files Archived by Mission Phase

Type	Description	CRU ^a	MOI ^b	MAP ^c
<i>Primary Data</i>				
ODR	original data record (open-loop)	124	1070	6026 ^d
TDF	tracking data file (closed-loop)	32	420	428
<i>Secondary Data</i>				
ODF	orbit data file	195	1253	624
<i>Ancillary Data</i>				
AGK	antenna gimbal kernel file	0	0	783
AMD	angular momentum desaturation file	84	922	682
ECH	spacecraft engineering data (channelized)	296	581	1391
ECS	engineering channel summary	5	5	1
ECT	engineering channel table	0	397	687
EOP	Earth orientation parameters	77	302	404
GDN	Goddard reconstructed trajectory file	0	148	285
ION	ionosphere media calibration file	50	97	123
IPN	JPL reconstructed trajectory file	0	0	10
LIT	light time file	8	39	4
MCH	channelized DSN monitor data	151	558	1389
MCT	monitor channel table	0	0	2165
MIF	maneuver implementation file	3	12	4
MPD	maneuver profile file	0	104	0
OPT	orbit propagation and timing file	0	539	331
SAK	solar array kernel	21	601	695
SFO	space flight operation sequence	22	712	0
SOE	sequence of events	22	987	434
SPK	spacecraft and planetary kernel	16	537	331
TCK	spacecraft orientation (CK) file	102	526	773
TRO	troposphere media calibration file	12	71	118
WEA	DSN weather file	98	243	299

^aCruise to Mars, Nov. 11, 1996 to Sept. 12, 1997.

^bMars Orbit Insertion, Sept. 12, 1997 to Mar. 9, 1999; includes gravity calibration orbit phase, Feb. 4–27.

^cMapping, Mar. 9, 1999, to Jan. 31, 2001.

^dAbout 85% of mapping orbit occultations are of very high quality, while the percentage of high-quality orbit insertion observations is much less. We estimate the total number (Jan. 31, 2001) of high quality observations to be ~ 5000 , although the useful number is somewhat higher.

surface to altitudes as high as 50 km where the pressure is ~ 3 Pa. Uncertainties in retrieved temperature and pressure near the surface are as low as 0.2%, or ~ 0.4 K and ~ 2 Pa, under the best observing conditions; at the top of the atmosphere the uncertainties increase to $\sim 7\%$, or roughly 10 K and 0.6 Pa. Although smoothed to a vertical resolution of several hundred meters, standard retrieved atmospheric parameters can be located on specified surfaces of the Mars' geopotential to within a few meters for purposes of comparing conditions at different locations. This latter capability, in conjunction with the low uncertainties of the retrieved parameters, makes it possible to use observations closely sampled in time and space to calculate a component of the absolute wind field from the gradient wind equation. The accuracy and coverage obtained with these observations supports studies of the large-scale structure and dynamics of the atmosphere, including the seasonal variations of the atmospheric fields and embedded waves, including tidal, Rossby, and Kelvin wave types. Two groups of observations, one providing systematic, rapid sampling of the meridional structure and the other providing close sampling of the zonal structure, illustrate the use of MGS occultations for these purposes. Mars general circulation models are an important adjunct to the use of the occultation results in the interpretation of these observations. On the other hand, the detailed structure provided by the occultation results is a constraint on the behavior of atmospheric models.

Results by *Hinson et al.* [1999, 2001] demonstrate these capabilities and provide new results for Mars' atmospheric dynamics. Atmospheric observations collected to date from the mapping orbit sample approximately one Mars year beginning at $L_s \approx 107^\circ$. These observations, together with additional measurements to be obtained in the remainder of the MGS mission, can be expected to provide new insights into the detailed mechanisms of the atmosphere.

Highly oblique scattering from the surface is routinely observed in connection with the occultation observations. Although some such scattering events were expected on the basis of Mariner and Viking experience, the fraction of occurrences was not anticipated to be large.

Appendix A: Data Product Summary

Tables A1 and A2 provide summary descriptions of the radio science data types, the acronyms by which these are known, and the number of files in the archive as of January 2001. Detailed documentation and copies of the files can be obtained in hard copy from the NASA Planetary Data System (PDS), or electronically from <http://wundow.wustl.edu/mgs/>; an alternative site is <http://atmos.nmsu.edu/mgsdata.html>. Primary raw data comprise the direct measurements of radio observables with essentially no corrections. Secondary raw data comprise only selected parameters from the complete tracking data set chosen for use by the MGS Navigation Team and RS gravity investigators. Corrections for various perturbation error sources (e.g., angular momentum dumps for the spacecraft reaction wheels) and geometric effects (e.g., motion of the spacecraft high gain antenna with respect to the spacecraft center of gravity) are generated from ancillary data. In addition, reduction of occultation observations to retrieve atmospheric structure requires orbit files describing the spacecraft position with respect to the center of mass of Mars. These are obtained in preliminary form from the MGS Navigation Team. Final data reduction requires a precision ephemeris, however, which is generated by the RS Team gravity investigators. These precision ephemeris files are included in the RS Raw Data Archive as Ancillary Data types GDN and IPN.

Raw data files are collected, edited, formatted, and written to CD-Rs as they are received from the MGS Project, DSN, and other sources. Approximately six

Table A2. Reduced Data Files Archived

Type	Description	Number of Files ^a
<i>Standard Products</i>		
RSTP	occultation temperature-pressure profiles	1103
OCCSUM	occultation summary files	5
SHA	spherical harmonic gravity models (ASCII files)	12
SHB	spherical harmonic gravity models (binary, with covariances)	5
RSDMAP	radio science digital map products (gravity)	17
LOSAPDR	line-of-sight acceleration profile	93
<i>Special Products</i>		
SRI	surface reflection images	1228
SRT	surface reflection tabular data	1228
SRI	surface reflection geometry summary	1228
EDS	ionospheric electron density profiles	32

^aNumber archived through January 31, 2001.

months after creation, each CD-R is delivered to the PDS; after validation by PDS, these files become generally available.

Standard and special reduced data types are released each 3 months. Solutions for the gravity field are based on tracking data accumulated over an extended period required to build up dense orbital coverage of the planet. The current solutions, which are based on data collected through late 2000, are included in the data listed in the tables. These products are revised when the solutions have improved significantly, approximately annually. A final global field model based on all the data will not be available until about a year after the end of data collection. The spatial resolution is not expected to increase much beyond the current limits, however, as it is constrained by the ~ 400 km altitude of the MGS orbit; resolving features much smaller than this is problematic.

Occultation results for the atmosphere are released at three month intervals. Early results were delayed by difficulties with the standard orbit solutions, which would have introduced unacceptable systematic errors. The only special products created to date are reduced results for scattering from the surface seen in the occultation data sets and standard resolution ionospheric electron density profiles.

By mission phase, total CD-R volumes written as of January 2001, include 56 from cruise, 159 from orbit insertion, and 184 from mapping.

Acknowledgments. We thank John Armstrong (JPL) for his contributions to the discussion of gravitational radiation and acknowledge his leading role in this aspect of the radio science investigation; F. Lemoine (GSFC), A. Konopliv (JPL), and D.-N. Yuan (JPL) made significant contributions to solution for the gravity field (see companion papers); S. Abatte (JPL/DSN) provided expert help in implementation and maintenance of the operational radio science ground system; M. Zuber contributed valuable discussions and suggestions throughout the course of the MGS mission; R. J. Wilson kindly supplied Viking lander surface pressures versus L_s ; C. S. Han provided helpful comments on the manuscript. We also thank two anonymous reviewers for substantive comments and helpful suggestions. This work is supported by NASA and the Mars Global Surveyor/Mars Surveyor Operations Project at JPL.

References

- Allan, D. W., Statistics of atomic frequency standards, *Proc. IEEE*, *54*, 221-230, 1966.
- Ahmad, B., and G. L. Tyler, The two-dimensional resolution kernel associated with retrieval of ionospheric and atmospheric refractivity profiles by Abelian inversion of radio occultation phase data, *Radio Sci.*, *33*, 129-142, 1998.
- Ahmad, B., and G. L. Tyler, Systematic errors in atmospheric profiles obtained from Abelian inversion of radio occultation data: Effects of large scale horizontal gradients, *J. Geophys. Res.*, *104*, 3971-3992, 1999.
- Albee, A., R. E. Arvidson, F. D. Palluconi, and T. E. Thorpe, Overview of the Mars Global Surveyor mission, *J. Geophys. Res.*, this issue.
- Armstrong, J. W., Radio wave phase scintillation and precision Doppler tracking of spacecraft, *Radio Sci.*, *33*, 1727-1738, 1998.
- Balmino, G., B. Moynot, and N. Vales, Gravity field model of Mars in spherical harmonics up to degree and order eighteen, *J. Geophys. Res.*, *87*, 9735-9746, 1982.
- Bass, F. G., and I. M. Fuks, *Wave Scattering from Statistically Rough Surfaces*, edited by C. B. Vesecky and J. F. Vesecky, Sects. 22-23, pp. 275-315, Pergamon, Tarrytown, N. Y., 1979.
- Beckmann, P., Shadowing of random rough surfaces, *IEEE Trans. Antennas Propag.*, *AP-13*, 384-388, 1965.
- Bills, B. G., The moments of inertia of Mars, *Geophys. Res. Lett.*, *16*, 385-388, 1989a.
- Bills, B. G., Comment on "More about the moment of inertia of Mars," *Geophys. Res. Lett.*, *16*, 1337-1338, 1989b.
- Conrath, B. J., J. C. Pearl, M. D. Smith, W. C. Maguire, P. R. Christensen, S. Dason, and M. S. Kaelberer, Mars Global Surveyor Thermal Emission Spectrometer (TES) observations: Atmospheric temperatures during aerobraking and science phasing, *J. Geophys. Res.*, *105*, 9509-9519, 2000.
- Estabrook, F. B., and H. D. Wahlquist, Response of Doppler spacecraft tracking to gravitational radiation, *Gen. Rel. Grav.*, *6*, 439-447, 1975.
- Fjeldbo, G., Bistatic-radar methods for studying planetary ionospheres and surfaces, Ph.D. Dissertation, 87 pp., Stanford Univ., Stanford, Calif., 1964.
- Fjeldbo, G., A. Kliore, and B. Seidel, Bistatic radar measurements of the surface of Mars with Mariner 1969, *Icarus*, *16*, 502-508, 1972.
- Folkner, W. M., R. D. Kahn, R. A. Preston, C. F. Yoder, E. M. Standish, J. G. Williams, C. D. Edwards, R. W. Hellings, T. M. Eubanks, and B. G. Bills, Mars dynamics from Earth-based tracking of the Mars Pathfinder Lander, *J. Geophys. Res.*, *102*, 4057-4064, 1997a.
- Folkner, W.M., C. F. Yoder, D.-N. Yuan, E. M. Standish, and R. A. Preston, Interior structure and seasonal mass redistribution of Mars from radio tracking of Mars Pathfinder, *Science*, *278*, 1749-1752, 1997b.
- Hagfors, T., Relations between rough surfaces and their scattering properties as applied to radar astronomy, in *Radar Astronomy*, edited by J. V. Evans and T. Hagfors, chap. 4, McGraw-Hill, New York, 1968.
- Hinson, D. P., R. A. Simpson, J. D. Twicken, G. L. Tyler, and F. M. Flasar, Initial results from radio occultation measurements with Mars Global Surveyor, *J. Geophys. Res.*, *104*, 26,997-27,012, 1999.
- Hinson, D. P., G. L. Tyler, J. L. Hollingsworth, and R. J. Wilson, Radio occultation measurements of forced atmospheric waves on Mars, *J. Geophys. Res.*, *106*, 1463-1480, 2001.
- Joshi, M., R. Haberle, J. Hollingsworth, and D. Hinson, A comparison of MGS Phase 1 aerobraking radio occultation data and the NASA Ames Mars GCM, *J. Geophys. Res.*, *105*, 17601-17615, 2000.
- Kaula, W. M., *Theory of Satellite Geodesy*, Blaisdell, Waltham, Mass., 1966.
- Kaula, W. M., N. H. Sleep, and R. J. Phillips, More about the moment of inertia of Mars, *Geophys. Res. Lett.*, *16*, 1333-1336, 1989.
- Kayarel, E. T., and D. P. Hinson, Sub-Fresnel-scale vertical resolution in atmospheric profiles from radio occultation, *Radio Sci.*, *32*, 411-423, 1997.
- Konopliv, A. S., and W. L. Sjogren, The JPL Mars gravity field, Mars50c, based upon Viking and Mariner 9 Doppler tracking data, *JPL Publ.*, *95-5*, 73 pp., 1995.
- Lemoine, F. G., et al., The Development of the Joint NASA GSFC and the National Imagery and Mapping Agency (NIMA) Geopotential Model EGM96, *Tech. Publ. NASA/*

- TP-1009-206861, 575 pp., Goddard Space Flight Cent., Greenbelt, Md., 1998.
- Lemoine, F. G., D. E. Smith, D. D. Rowlands, M. T. Zuber, G. A. Neumann, and D. S. Chinn, Improved solutions of the gravity field of Mars from Mars Global Surveyor, (abstract), *Eos Trans. AGU*, 81(19), Spring Meet. Suppl., S299, 2000.
- Lemoine, F. G., D. E. Smith, D. D. Rowlands, M. T. Zuber, G. A. Neuman, D. S. Chinn, and D. E. Pavlis, An improved solution of the gravity field of Mars (GMM-2B) from Mars Global Surveyor, *J. Geophys. Res.*, this issue.
- Morabito, D., S. Butman, and S. Shambayati, The Mars Global Surveyor Ka-band Link Experiment (MGS/KABLE-II), in *The Telecommunications and Data Acquisition Progress Rep. 42-137*, Jet Propul. Lab., Pasadena, Calif., May 15, 1999.
- Ogilvy, J. A., *Theory of Wave Scattering From Random Rough Surfaces*, Adam Hilger, Bristol, 1991.
- Phillips, R. J., et al., Ancient geodynamics and global-scale hydrology on Mars, *Science*, 291, 2587–2591, 2001.
- Reasenber, R. D., The moment of inertia and isostasy of Mars, *J. Geophys. Res.*, 82, 369–375, 1977.
- Sancer, M. L., Shadow-corrected electromagnetic scattering from a randomly rough surface, *IEEE Trans. Antennas Propag.*, AP-17, 577–585, 1969.
- Sjogren, W. L., Mars Gravity: High-resolution results from Viking Orbiter 2, *Science*, 203, 1006–1010, 1979.
- Smith, D. E., F. J. Lerch, J. C. Chan, D. S. Chinn, H. B. Iz, A. Mallama, and G. B. Patel, Mars gravity field error analysis from simulated radio tracking of Mars Observer, *J. Geophys. Res.*, 95, 14,155–14,167, 1990.
- Smith, D. E., F. J. Lerch, R. S. Nerem, M. T. Zuber, G. B. Patel, S. K. Fricke, and F. J. Lemoine, An improved gravity field for Mars: Goddard Mars Model-1 (GMM-1), *J. Geophys. Res.*, 98, 20,871–20,889, 1993.
- Smith, D. E., F. G. Lemoine, M. T. Zuber, Simultaneous estimation of the masses of Mars, Phobos, and Deimos using spacecraft distant encounters, *Geophys. Res. Lett.*, 22, 2171–2174, 1995.
- Smith, D. E., W. L. Sjogren, G. L. Tyler, G. Balmino, F. G. Lemoine, and A. S. Konopliv, The gravity field of Mars: Results from Mars Global Surveyor, *Science*, 286, 94–97, 1999a.
- Smith, D. E., M. T. Zuber, R. M. Haberle, D. D. Rowlands, J. R. Murphy, The Mars seasonal CO₂ cycle and the time variation of the gravity field: A general circulation model simulation, *J. Geophys. Res.*, 104, 1885–1896, 1999b.
- Smith, D. E., et al., The global topography of Mars and implications for surface evolution, *Science*, 284, 1495–1503, 1999c.
- Smith, D. E., M. T. Zuber, P. J. Dunn, M. H. Torrence, S. K. Fricke, Observed changes in the gravity field of Mars due to seasonal atmospheric processes (abstract), *Eos Trans. AGU*, 81(48), Fall Meet. Suppl., F316, 2000.
- Smith, D. E., et al. Mars Orbiter Laser Altimeter: Experiment summary after the first year of global mapping of Mars, *J. Geophys. Res.*, this issue.
- Smith, M. D., J. C. Pearl, B. J. Conrath, and P. R. Christensen, Mars Global Surveyor Thermal Emission Spectrometer (TES) observations of dust opacity during aerobraking and science phasing, *J. Geophys. Res.*, 105, 9539–9552, 2000.
- Thorne, K. S., Gravitational Radiation, in *300 Years of Gravitation*, edited by S. W. Hawking and W. Israel, pp. 338–345, Cambridge Univ. Press, New York, 1987.
- Tinto, M., and J. W. Armstrong, Spacecraft Doppler tracking as a narrow-band detector of gravitational radiation, *Phys. Rev. D Part. Fields*, 58, 042002/1-8, 1998.
- Turcotte, D. L., R. J. Willeman, W. F. Haxby, and J. Norberry, Role of membrane stresses in the support of planetary topography, *J. Geophys. Res.*, 86, 3951–3959, 1981.
- Tyler, G. L., Radio propagation experiments in the outer solar system with Voyager, *Proc. IEEE*, 75, 1404–1431, 1987.
- Tyler, G. L., G. Balmino, D. P. Hinson, W. L. Sjogren, D. E. Smith, R. T. Woo, S. W. Asmar, M. J. Connally, C. L. Hamilton, and R. A. Simpson, Radio science investigations with Mars Observer, *J. Geophys. Res.*, 97, 7759–7779, 1992.
- Vesecky, J. F., Electromagnetic wave scattering from a gently undulating, rough surface at near grazing incidence, in *Proceedings of the DARPA Low-Angle Tracking Symposium, I*, pp. 39–62, Def. Adv. Res. Proj. Agency, Santa Barbara, Calif., 1977.
- Vesecky, J. F., E. J. Sperley, and H. Zebker, Electromagnetic wave scattering at near-grazing incidence from a gently undulating, rough surface, in *Proceedings of the International Geoscience and Remote Sensing Symposium*, pp. 1579–1583, Inst. of Elect. and Electron. Eng., New York, 1988.
- Yuan, D.-N., W. L. Sjogren, A. S. Konopliv, and A. B. Kucinskis, Gravity field of Mars: A 75th degree and order model, *J. Geophys. Res.*, this issue.
- Zuber, M. T., S. C. Solomon, R. J. Phillips, D. E. Smith, G. L. Tyler, O. Aharonson, G. Balmino, W. B. Brainerdt, J. W. Head, C. L. Johnson, F. G. Lemoine, P. J. McGovern, G. A. Neuman, D. D. Rowlands, and S. Zhong, Internal structure and early thermal evolution of Mars from Mars Global Surveyor topography and gravity, *Science*, 287, 1788–1793, 2000.
- Zurek, R. W., J. R. Barnes, R. M. Haberle, J. B. Pollack, J. E. Tillman, and C. B. Leovy, Dynamics of the atmosphere of Mars, in *Mars*, edited by H. H. Kieffer et al., chap. 26, Univ. of Ariz., Tucson, 1992.

S. W. Asmar and W. L. Sjogren, Jet Propulsion Laboratory, 4800 Oak Grove Drive, Pasadena, CA 91109. (sami.asmar@jpl.nasa.gov; wls@nomad.jpl.nasa.gov)

G. Balmino, Centre National d'Etudes Spatiales, GRGS-18, Avenue Edouard Belin, 31401 Toulouse Cedex 4, France. (georges.balmino@cnes.fr)

D. P. Hinson, R. A. Simpson, J. D. Twicken, and G. L. Tyler, Space, Telecommunications, and Radio Science Laboratory, 350 Serra Mall, Stanford University, Stanford, CA 94305-9515. (hinson@nimbus.stanford.edu; rsimpson@magellan.stanford.edu; len.tyler@stanford.edu; joe@nova.stanford.edu)

P. Priest, 30/2056, Microsoft Corporation, One Microsoft Way, Redmond, WA 98052. (trishp@microsoft.com)

D. E. Smith, Code 920.0, NASA Goddard Space Flight Center, Greenbelt, MD 20771. (dsmith@tharsis.gsfc.nasa.gov)

(Received August 7, 2000; revised February 26, 2001; accepted March 16, 2001.)